

Brown Dwarf Candidates in the JADES and CEERS Extragalactic Surveys

KEVIN N. HAINLINE ¹, JAKOB M. HELTON ¹, BENJAMIN D. JOHNSON ², FENGWU SUN ¹, MICHAEL W. TOPPING ¹,
JARRON M. LEISENRING ¹, WILLIAM M. BAKER ^{3,4}, DANIEL J. EISENSTEIN ², RYAN HAUSEN ⁵,
RAPHAEL E. HVIDING ¹, JIANWEI LYU ¹, BRANT ROBERTSON ⁶, SANDRO TACCHIELLA ^{3,4},
CHRISTINA C. WILLIAMS ⁷, CHRISTOPHER N. A. WILLMER ¹ AND THOMAS L. ROELLIG ⁸

¹*Steward Observatory, University of Arizona, 933 N. Cherry Ave, Tucson, AZ 85721, USA*

²*Center for Astrophysics | Harvard & Smithsonian, 60 Garden St., Cambridge MA 02138 USA*

³*Kavli Institute for Cosmology, University of Cambridge, Madingley Road, Cambridge CB3 0HA, UK*

⁴*Cavendish Laboratory, University of Cambridge, 19 JJ Thomson Avenue, Cambridge CB3 0HE, UK*

⁵*Department of Physics and Astronomy, The Johns Hopkins University, 3400 N. Charles St. Baltimore, MD 21218*

⁶*Department of Astronomy and Astrophysics, University of California, Santa Cruz, 1156 High Street, Santa Cruz CA 96054, USA*

⁷*NSF's National Optical-Infrared Astronomy Research Laboratory, 950 North Cherry Avenue, Tucson, AZ 85719, USA*

⁸*NASA Ames Research Center, MS 245-6, Moffett Field, CA 94035, USA*

ABSTRACT

By combining the JWST/NIRCam JADES and CEERS extragalactic datasets, we have uncovered a sample of twenty-one T and Y brown dwarf candidates at best-fit distances between 0.1 - 4.2 kpc. These sources were selected by targeting the blue $1\mu\text{m} - 2.5\mu\text{m}$ colors and red $3\mu\text{m} - 4.5\mu\text{m}$ colors that arise from molecular absorption in the atmospheres of $T_{\text{eff}} < 1300\text{K}$ brown dwarfs. We fit these sources using multiple models of substellar atmospheres and present the resulting fluxes, sizes, effective temperatures and other derived properties for the sample. If confirmed, these fits place the majority of the sources in the Milky Way thick disk and halo. We observe proper motion for seven of the candidate brown dwarfs with directions in agreement with the plane of our Galaxy, providing evidence that they are not extragalactic in nature. We demonstrate how the colors of these sources differ from selected high-redshift galaxies, and explore the selection of these sources in planned large-area JWST NIRCam surveys. Deep imaging with JWST/NIRCam presents an excellent opportunity for finding and understanding these ultracool dwarfs at kpc distances.

Keywords: Brown dwarfs(185) — Halo stars(699) — Infrared astronomy(786) — James Webb Space Telescope(2291)

1. INTRODUCTION

At the intersection of stellar and exoplanet science lies the study of ultracool brown dwarfs, low-mass objects ($M < 0.07 M_{\odot}$) at relatively cool effective temperatures ($T_{\text{eff}} < 2500\text{K}$). Over the last several decades researchers have uncovered many hundreds of brown dwarfs, which extend the stellar classification system from hot O-type stars down to L ($T_{\text{eff}} = 1300 - 2000\text{K}$), T ($T_{\text{eff}} = 700 - 1300\text{K}$), and Y ($T_{\text{eff}} < 700\text{K}$) dwarfs (Kirkpatrick et al. 1999; Cushing et al. 2011; Kirkpatrick et al. 2021). Selecting and characterizing these sources is vital for exploring the stellar/substellar initial mass function, understanding binary stellar evolution, and for increasing the census of stars around which potentially habitable planets may lie.

However, at very low temperatures, brown dwarfs emit most of their flux in the infrared (IR) and are optically quite faint with spectral energy distributions (SEDs) that feature broad molecular and narrow resonance features (from H_2O , CH_4 , NH_3 , CO , and CO_2 , among others). The observational depths for existing large area IR surveys restrict the recovered brown dwarfs to those in the Solar Neighborhood, although there are individual sources that have been found in the Milky Way thick disk and halo (Burgasser et al. 2003b; Lodieu et al. 2010; Murray et al. 2011; Burningham et al. 2014; Zhang et al. 2019; Schneider et al. 2020). It is vital to expand on these samples, as brown dwarfs at these distances help us understand the history of star formation in the Milky Way.

Low-temperature brown dwarf candidates have been serendipitously discovered in deep near-IR surveys from the Hubble Space Telescope (HST), as they serve as a potential contaminant in the search for high-redshift galaxies and quasars (Bunker et al. 2004; Wilkins et al. 2014; Finkelstein et al. 2015; Bouwens et al. 2015; Bañados et al. 2016). Several authors have used the accumulated area of multiple deep HST near-IR surveys to perform systematic searches for brown dwarf candidates with observations out to $\sim 2\mu\text{m}$ (Ryan et al. 2011; Masters et al. 2012; Aganze et al. 2022). Models of brown dwarf emission, however, show that while they do emit at 1 - $2\mu\text{m}$, cold T and Y dwarfs peak at 4 - $5\mu\text{m}$, outside of the wavelength coverage by HST, with faint fluxes requiring very deep observations.

With the launch of the James Webb Space Telescope (JWST), a new chapter in finding low-mass stars and brown dwarfs has begun. The NIRC*am* instrument on JWST offers imaging across a FOV of 9.7 arcmin^2 at $0.7 - 5.0\mu\text{m}$ in the near-IR. Current and upcoming extragalactic surveys, which will cover tens to many hundreds of square arcminutes, will explore flux limits ideal for selecting cold brown dwarfs (Holwerda et al. 2018; Hainline et al. 2020). Indeed, multiple studies have predicted the number counts of brown dwarfs in JWST deep surveys (Ryan & Reid 2016; Aganze et al. 2022; Casey et al. 2022), and in the first year of JWST, there have been discoveries made of individual brown dwarf candidates in both the JWST Director’s Discretionary Early Release Science Program ERS 1324, GLASS, (Nonino et al. 2023) and the Cosmic Evolution Early Release Science (CEERS) Survey (Wang et al. 2023). Excitingly, Langeroodi et al. (2023) and Burgasser et al. (2023) both independently confirmed a number of brown dwarf candidates using spectroscopy taken as part of the Ultra-deep NIRC*am* and NIRS*pec* Observations Before the Epoch of Reionization (UNCOVER, Bezanson et al. 2022), including the source from Nonino et al. (2023). These spectroscopic confirmations demonstrate the usage of deep extragalactic data for finding these rare sources. It should be noted that deep fields are chosen to point away from the disk of the Milky Way to avoid stellar contamination, and as a result the populations of brown dwarfs observed in these surveys may not be broadly applicable to the full Milky Way population.

Following these studies, we aim to use the JWST Advanced Deep Extragalactic Survey (JADES) observations (Eisenstein et al. 2023a) of the Great Observatories Origins Deep Survey (GOODS) Southern and Northern regions (Giavalisco et al. 2004) to explore the brown dwarf population at $T_{\text{eff}} < 1300\text{K}$. These data, which we combine with deep ancillary HST observations

at optical wavelengths, probe near-IR depths down to 29 - 30th magnitude AB. In addition, we supplement these observations with NIRC*am* observations from the CEERS Survey (Finkelstein et al. 2022) to increase the area covered at similar observational depths. Sources detected in these surveys offer a unique opportunity to understand brown dwarfs at kpc distances in the Milky Way thick disk and halo, and can be used to explore the types of subdwarf populations that will be observed in future very large area JWST surveys such as COSMOS-Web (Casey et al. 2022) and PRIMER (Dunlop et al. 2021).

The outline of this paper is as follows. In Section 2 we discuss the JADES and CEERS data we are using for finding brown dwarf candidates, the reduction of these data, and the extraction of photometry. We then describe the selection procedure for separating substellar candidates from galaxies. In Section 3 we present our full sample of 21 brown dwarf candidates, discuss our brown dwarf model fitting procedure, and the recovered properties of these objects, including their temperatures and distances. We also describe the measured proper motions for a subset of our sources. In Section 4 we explore the positions of these sources within the Galaxy, demonstrate methods to separate these sources from high-redshift galaxy candidates, and discuss the selection of brown dwarfs in other JWST deep extragalactic surveys. Finally, we conclude in Section 5. Throughout this paper we will be using magnitudes in the AB system (Oke 1974).

2. DATA AND SAMPLE

2.1. JWST NIRC*am* Observations

In order to explore the types of brown dwarf candidates that can be recovered in deep extragalactic fields, we looked at both the JADES and CEERS datasets, which consist of deep NIRC*am* observations in multiple filters spanning $1 - 5\mu\text{m}$ that we use to separate these sources from galaxies. These survey data have been explored both to find (Finkelstein et al. 2022; Robertson et al. 2023; Hainline et al. 2023) and spectroscopically-confirm (Curtis-Lake et al. 2023; Arrabal Haro et al. 2023; Fujimoto et al. 2023) the farthest high-redshift galaxies as of the writing, making them ideal fields for understanding the role of brown dwarf contamination of extragalactic samples.

2.1.1. JADES

JADES is an observing program that combines data from the NIRC*am* and NIRS*pec* extragalactic Guaranteed Time Observations (GTO) teams. The final data set includes NIRC*am* and MIRI imaging with NIRS*pec*

spectroscopy across two well-studied fields: GOODS-S (RA = 53.126 deg, DEC = -27.802 deg) and GOODS-N (RA = 189.229, DEC = +62.238 deg). For this study, we focus on the NIRCcam observations taken as of February 8 2023. The observations and reduction of the JADES data we use in this study are fully described in Eisenstein et al. (2023a). Briefly, we use the JADES NIRCcam observations taken as part of JWST PID 1180 and 1181 (PI:Eisenstein), as well as PID 1210 and 1286 (PI:Ferruit).

In total, the JADES GOODS-S area is 67 square arcminutes, with 27 square arcminutes for the JADES Deep program, and 40 square arcminutes for the JADES Medium program. The filters used for the JADES Deep program in GOODS-S are NIRCcam F090W, F115W, F150W, F200W, F277W, F335M, F356W, F410M, and F444W ($\lambda = 0.8 - 5.0\mu\text{m}$), and the JADES Medium area was observed with the same filters, but without F335M. For the NIRCcam parallel to the NIRSpec 1286 program, the F070W filter was included. The JADES GOODS-N area is 58 square arcminutes, split into a deeper southeast (SE) portion (27.6 square arcminutes) and a relatively shallower northwest (NW) portion (30.4 square arcminutes). For the GOODS-N observations, the filters used were F090W, F115W, F150W, F200W, F277W, F335M, F356W, F410M, and F444W, similar to JADES Deep in GOODS-S.

We supplement the JADES observations with data from the publicly available JWST Extragalactic Medium Survey (JEMS, Williams et al. 2023), which focuses on the center of the JADES Deep region and uses NIRCcam filters F182M, F210M, F430M, F460M, and F480M. In addition, we include F444W observations from the The First Reionization Epoch Spectroscopic COmplete Survey (FRESCO, PID 1895, Oesch et al. 2023). As part of this NIRCcam grism survey of the GOODS-S and GOODS-N fields, NIRCcam imaging was obtained in the F182M, F210M, and F444W filters. We combine the F444W imaging from the FRESCO data with the JADES imaging in the region where the surveys overlap. The 5σ point-source depths in a $0.2''$ diameter circular aperture vary across the fields and filters between 28.8 and 30.6 AB Mag (see Eisenstein et al. 2023a, for more details).

At shorter wavelengths, to uncover potential proper motions, we also use existing HST/ACS and WFC3 mosaics. We use the HST/ACS and HST/WFC3 mosaics from the Hubble Legacy Fields (HLF) v2.0 for GOODS-S and v2.5 for GOODS-N ($25' \times 25'$ for GOODS-S, and $20.5' \times 20.5'$ for GOODS-N, Illingworth et al. 2013; Whitaker et al. 2019). We use data in the HST/ACS F435W, F606W, F775W, F814W, and F850LP filters to

aid in exploring galaxy fits, and HST/WFC3 F105W, F125W, F140W, and F160W for exploring proper motions.

Details of the data reduction and flux extraction are described in Robertson et al. (2023), Tacchella et al. (2023), and Eisenstein et al. (2023a). To select the brown dwarfs across the JADES survey, we use $0.2''$ diameter circular aperture magnitudes extracted from images that have been convolved to match the F444W point-spread function (PSF) to obtain accurate colors. We applied aperture corrections to these magnitudes using empirical JWST/NIRCcam PSFs assuming point source morphologies for our sources (see Ji et al. 2023, for more details). We note that the PSFs used in this analysis were derived from pre-flight pointing predictions.

2.1.2. CEERS

To supplement our sample of brown dwarf candidates, we additionally explore The Cosmic Evolution Early Release Science (CEERS) Survey¹ (Finkelstein et al. 2022) NIRCcam observations. The CEERS Survey currently targets 90.8 square arcminutes of the Extended Groth Strip (EGS) with the NIRCcam filters F115W, F150W, F200W, F277W, F356W, F410M, and F444W down to 5σ point-source depths of 28.4 - 29.3 AB Mag in a $0.2''$ diameter circular aperture. We combine the JWST data with public HST/ACS data covering the EGS in F606W and F814W (A. Koekemoer, private comm.). We used the reduction process outlined above on the raw CEERS observations, and again, chose the $0.2''$ diameter circular aperture magnitudes extracted from F444W PSF-convolved images to select sources.

2.2. Selecting Brown Dwarf Candidates

The first of the brown dwarf candidates were found serendipitously as part of the search for high-redshift galaxies presented in Hainline et al. (2023). These sources were observed with red NIRCcam F090W-F115W colors (similar to F090W Lyman dropout galaxies), blue F115W - F277W colors, and then exceedingly red F277W - F444W colors, producing a “V”-shaped SED. In addition, these sources had point-like morphologies, often with diffraction spikes from the NIRCcam PSF observed at long wavelengths. When we fits these sources with observed and simulated galaxy templates using the photometric redshift code EAZY (Brammer et al. 2008) following the procedure outlined in Hainline et al. (2023), the fits were generally very poor, with large χ^2 results for the best fits. The galaxy templates that we

¹ <https://ceers.github.io/>

used included both star-forming and quiescent sources, including those with very strong nebular continuum and line emission, and we allowed EAZY to combine all of the individual templates when fitting a given source. While galaxy templates could not reproduce the colors of these sources, they were quite similar to the very low temperature T dwarfs collected as part of the SpeX Prism Spectral Libraries², as well as the simulated brown dwarf SEDs from Marley et al. (2021) and Karalidi et al. (2021).

To better understand these interesting brown dwarf candidates, we performed a search across the JADES and CEERS footprints based on the colors of the objects serendipitously discovered as well as the colors of brown dwarfs in the literature. In Nonino et al. (2023), the authors selected a brown dwarf candidate from the JWST GLASS survey with $m_{F444W,AB} \leq 28$, $F356W-F444W \geq 1.5$ and $F115W-F444W \geq 2$, criteria that were chosen based on T and Y dwarf infrared colors presented in Meisner et al. (2020). For our search, we extended this selection down to $m_{F444W,AB} \leq 28.5$ due to the increased depth of the JADES and CEERS survey data, and in addition, we explored two alternate color selection schemes: $F277W-F444W \geq 0.0$ combined with either $F115W-F277W \leq 1.0$ or $F115W-F150W \leq 1.0$. These two selection criteria were designed to probe the “V”-shaped SED of these brown dwarf candidates, and were chosen based on the positions of the JADES galaxies and the colors of the Marley et al. (2021) and Karalidi et al. (2021) substellar atmospheric models.

We find 134 unique sources are selected by any one of the three color selection criteria in GOODS-S ($2.0/\text{arcmin}^2$), 173 ($3.0/\text{arcmin}^2$) in GOODS-N, and 355 ($3.9/\text{arcmin}^2$) across the CEERS survey data. The increased density of selected sources in GOODS-N and CEERS is due to the decreased observational depth, as for shallower surveys, noise preferentially scatters sources into the selection boxes. Additionally, we observe an increased number of hot pixels in the GOODS-N and CEERS datasets, often seen in the NIRCcam LW channel, boosting the observed F444W flux.

After making our photometry and color cuts, we examined the resulting samples of objects and rejected non-astrophysical sources, including hot pixels in the F444W mosaic and diffraction spikes from bright stars in the footprint. We also rejected sources with obvious extended morphologies, as those are likely galaxies. To further aid in removing potential galaxies, our candidate selection also required that the EAZY galaxy fit had

$\chi^2 > 20$. One source, CEERS-EGS-BD-5, has an EAZY galaxy fit with $\chi^2 = 18.31$, but we included this source in our final sample as the EAZY fit is not consistent with the non-detections in the ACS F606W and F814W filters. We rejected those sources with red long-wavelength slopes similar to those described in Furtak et al. (2022); Endsley et al. (2022); Barro et al. (2023); Labbé et al. (2023); Labbe et al. (2023); Matthee et al. (2023); Hainline et al. (2023), as these have colors inconsistent with brown dwarf models.

Our final sample consists of 11 sources in GOODS-S, 3 sources in GOODS-N, and 7 sources in CEERS, for a total of 21 brown dwarf candidates. For these candidates, we re-fit the photometry using *forcepho* (BDJ in prep), a modeling code that combines Sérsic profiles to measure the pixel-level fluxes for a given source directly from the individual NIRCcam exposures. The usage of *forcepho* on NIRCcam data is described in Robertson et al. (2023). The *forcepho* photometry agrees with the photometry used to select the original sources to within 3 – 26% varying between the filters (the F410M fluxes are the most discrepant, with the *forcepho* fluxes being systematically brighter than those measured with a circular aperture), and none of the *forcepho* colors for these sources are outside the selection criteria we used to initially select them. We impose a $\text{SNR} < 20$ limit on the *forcepho* uncertainties to account for systematics.

In Wang et al. (2023), the authors present a brown dwarf candidate selected from CEERS public data. In our independent reduction of the same dataset, we extracted flux for this source and found that the photometric measurements presented in their Table 1 are highly discrepant from our measurements. They present an AB magnitude in the F277W filter for this source of 29.02, while we measure a $0.2''$ diameter circular aperture magnitude in the same filter of 27.53 ± 0.04 . A separate photometric catalog from the The DAWN JWST Archive³ for the source includes a $0.36''$ diameter circular aperture magnitude of 27.37 ± 0.05 . In addition, the NIRCcam colors of the source as presented in Wang et al. (2023) are different from what we measure - we would not select this source based on our color criteria previously described. We are confident, based on the provided RA and DEC and the individual filter thumbnails presented in Wang et al. (2023) for the source, that we were comparing to the same object within our own reduction of the catalog. The EAZY fit to our measured fluxes for this object results in a fit at a photometric redshift $z_a = 5.9$ with $\chi^2 = 2.4$. Given that in our own reduction of these

² <https://cass.ucsd.edu/~ajb/browndwarfs/spexprism/index.html>

³ <https://dawn-cph.github.io/dja/>

Table 1. Brown Dwarf Candidate *forcePho* Fluxes (nJy)

Object ID	RA	DEC	$r_{\text{half}}(\prime)$	F090W	F115W	F150W	F200W
JADES-GS-BD-1	53.026024	-27.867171	0.001	37.06 ± 1.85	267.43 ± 13.37	139.33 ± 6.97	92.14 ± 4.61
JADES-GS-BD-2	53.036286	-27.883739	0.001	18.83 ± 1.09	115.93 ± 5.8	67.78 ± 3.39	41.41 ± 2.07
JADES-GS-BD-3	53.056307	-27.868408	0.002	0.35 ± 0.6	11.36 ± 0.58	4.81 ± 0.45	2.27 ± 0.51
JADES-GS-BD-4	53.076738	-27.889947	0.003	-1.46 ± 0.01	1.91 ± 0.47	1.76 ± 0.51	-0.16 ± 0.01
JADES-GS-BD-5	53.084040	-27.839348	0.001	0.09 ± 0.16	2.99 ± 0.15	1.91 ± 0.13	1.25 ± 0.17
JADES-GS-BD-6	53.103912	-27.908507	0.002	3.24 ± 0.66	25.58 ± 1.28	13.02 ± 0.67	5.66 ± 0.59
JADES-GS-BD-7	53.105547	-27.815154	0.001	12.98 ± 0.94	118.67 ± 5.93	58.75 ± 2.94	33.5 ± 1.68
JADES-GS-BD-8	53.133756	-27.825521	0.003	-1.09 ± 0.01	4.14 ± 0.39	0.86 ± 0.44	0.14 ± 0.39
JADES-GS-BD-9	53.161140	-27.809163	0.001	1.4 ± 0.32	17.11 ± 0.86	9.1 ± 0.46	3.63 ± 0.34
JADES-GS-BD-10	53.161800	-27.831613	0.001	305.8 ± 15.29	2330.96 ± 116.55	1313.29 ± 65.66	934.8 ± 46.74
JADES-GS-BD-11	53.200319	-27.764118	0.002	3.24 ± 0.87	34.55 ± 1.73	20.0 ± 1.0	5.95 ± 0.71
JADES-GN-BD-1	189.036189	62.234159	0.003	5.21 ± 1.74	40.12 ± 2.17	16.42 ± 1.7	8.83 ± 1.18
JADES-GN-BD-2	189.118004	62.268968	0.002	3.89 ± 1.25	26.68 ± 1.33	12.26 ± 1.08	4.53 ± 0.99
JADES-GN-BD-3	189.204787	62.245553	0.003	4.01 ± 1.48	74.93 ± 3.75	33.08 ± 1.65	14.5 ± 1.23
CEERS-EGS-BD-1	214.767936	52.845299	0.004	-	8.97 ± 0.83	3.53 ± 0.97	0.59 ± 0.9
CEERS-EGS-BD-2	214.823254	52.874531	0.004	-	8.89 ± 0.88	4.76 ± 0.98	1.81 ± 0.83
CEERS-EGS-BD-3	214.851340	52.799294	< 0.001	-	289.62 ± 14.48	138.55 ± 6.93	78.11 ± 3.91
CEERS-EGS-BD-4	214.910274	52.860077	0.002	-	81.6 ± 4.08	38.49 ± 1.92	29.99 ± 1.5
CEERS-EGS-BD-5	214.913696	52.895919	0.002	-	17.05 ± 0.85	8.55 ± 1.07	6.54 ± 0.94
CEERS-EGS-BD-6	214.940850	52.907711	0.003	-	3.28 ± 0.64	2.69 ± 0.92	0.05 ± 0.68
CEERS-EGS-BD-7	214.951604	52.913456	0.003	-	13.67 ± 0.68	7.38 ± 1.0	3.79 ± 0.69

Object ID	F277W	F335M	F356W	F410M	F444W
JADES-GS-BD-1	51.18 ± 2.56	-	131.92 ± 6.6	427.53 ± 21.38	327.93 ± 16.4
JADES-GS-BD-2	23.72 ± 1.19	19.04 ± 0.95	65.16 ± 3.26	178.97 ± 8.95	129.29 ± 6.46
JADES-GS-BD-3	-0.01 ± 0.01	-	6.52 ± 0.59	26.35 ± 1.74	19.67 ± 1.06
JADES-GS-BD-4	-0.23 ± 0.01	-	3.59 ± 0.6	21.73 ± 1.24	24.04 ± 1.2
JADES-GS-BD-5	8.77 ± 0.44	2.17 ± 0.47	60.25 ± 3.01	482.67 ± 24.13	624.61 ± 31.23
JADES-GS-BD-6	4.25 ± 0.81	-	15.69 ± 0.84	55.39 ± 2.77	43.55 ± 2.18
JADES-GS-BD-7	20.3 ± 1.28	-	66.83 ± 3.34	242.62 ± 12.13	209.54 ± 10.48
JADES-GS-BD-8	0.96 ± 0.54	-1.23 ± 0.01	6.52 ± 0.54	47.2 ± 2.36	49.2 ± 2.56
JADES-GS-BD-9	3.0 ± 0.32	1.72 ± 0.62	13.81 ± 0.69	53.26 ± 2.66	44.22 ± 2.35
JADES-GS-BD-10	559.6 ± 27.98	344.54 ± 17.23	1317.24 ± 65.86	4082.01 ± 204.1	2994.17 ± 149.71
JADES-GS-BD-11	7.55 ± 0.47	4.07 ± 1.13	50.98 ± 2.55	206.26 ± 10.31	172.51 ± 8.63
JADES-GN-BD-1	6.95 ± 1.34	-	33.03 ± 1.65	185.23 ± 9.26	183.02 ± 9.15
JADES-GN-BD-2	3.04 ± 1.13	-2.09 ± 0.01	18.03 ± 1.16	86.01 ± 4.3	69.02 ± 3.45
JADES-GN-BD-3	17.99 ± 1.22	8.86 ± 1.96	107.81 ± 5.39	643.26 ± 32.16	638.52 ± 31.93
CEERS-EGS-BD-1	0.4 ± 1.24	-	7.22 ± 1.19	31.04 ± 2.97	25.53 ± 2.64
CEERS-EGS-BD-2	1.12 ± 1.0	-	10.52 ± 1.28	61.99 ± 3.18	50.82 ± 2.54
CEERS-EGS-BD-3	61.89 ± 3.09	-	143.33 ± 7.17	478.62 ± 23.93	389.8 ± 19.49
CEERS-EGS-BD-4	14.22 ± 0.74	-	35.32 ± 1.8	146.27 ± 7.31	115.95 ± 5.8
CEERS-EGS-BD-5	2.7 ± 1.08	-	8.89 ± 1.02	34.09 ± 2.81	22.37 ± 2.45
CEERS-EGS-BD-6	0.21 ± 1.29	-	4.63 ± 0.93	28.56 ± 3.13	33.92 ± 2.56
CEERS-EGS-BD-7	2.9 ± 1.51	-	8.6 ± 1.0	60.33 ± 3.7	59.95 ± 3.0

data this source would not be selected as a brown dwarf candidate, we do not include it in our analysis.

In Figure 1, we plot the color selection regions that we used for selecting our candidates. In each panel, we represent the colors for the JADES sources measured using the $0.2''$ diameter circular aperture magnitudes with a greyscale density plot. The final sample of JADES and CEERS candidates is plotted with red points. We compare our candidates to the colors for the ‘‘Sonora Cholla’’ brown dwarf model atmospheres from Karalidi

et al. (2021). We plot the solar metallicity Sonora Cholla points with colors shaded by the model effective temperature. We find that most of our sources would not be selected by the color criteria used in Nonino et al. (2023), as shown in the left panel of Figure 1. These color limits would only select Sonora Cholla models with effective temperature $T_{\text{eff}} < 700\text{K}$ (Y dwarfs). The selection criteria depicted in the middle and right panels of Figure 1, on the other hand, includes the majority of the brown dwarf Sonora Cholla model points across the full range

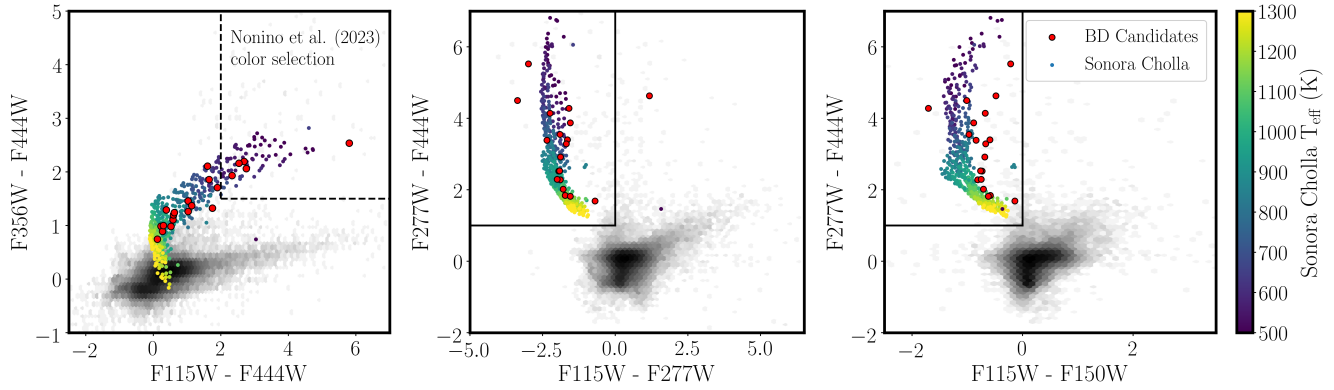


Figure 1. Color criteria used to select brown dwarf candidates in this work. In each panel, JADES sources with $m_{F444W} < 28.5$ are plotted in grey. Our selected JADES and CEERS candidates discussed in this paper are shown with red circles with black outlines, and the predicted ultracool dwarf colors from the Sonora Cholla models are plotted with small points colored by the T_{eff} values as shown in the colorbar. The black lines represent the color limits used for selecting sources. *Left:* F356W - F444W color plotted against F115W - F444W color, with dashed black lines showing the color criteria adopted by (Nonino et al. 2023) for selecting their brown dwarf candidate in the JWST GLASS data. These colors would limit the resulting Sonora Cholla brown dwarf models to those with $T_{\text{eff}} < 700\text{K}$. *Middle:* F277W - F444W color plotted against F115W - F277W color, with the color limits used in selecting sources represented with solid lines. *Right:* F277W - F444W color plotted against F115W - F150W color, with the color limits used in selecting sources represented with solid lines. Both the middle and right panels feature new color criteria designed to recover the “V”-shaped SED seen in brown dwarf models from Marley et al. (2021) and Karalidi et al. (2021).

of modeled T_{eff} values, and separates these sources from the bulk of the JADES galaxies. Our candidates have colors that nicely agree with the Sonora Cholla model colors, although one object, JADES-GS-BD-5, lies outside of the F277W-F444W vs. F115W-F277W selection box by virtue of its red F115W - F277W color. This source will be discussed further in the next section.

To estimate the brown dwarf properties, including the distances to these candidates, we fit the NIRC*am* *forcepho* fluxes for the sources with the Karalidi et al. (2021) Sonora Cholla models. We do not fit the HST ACS or WFC3 fluxes because of the possibility of proper motion making it difficult to assure that the measured flux corresponds to the correct source (see the next section for a discussion of the sources with observed proper motion). The models are provided with three free parameters: effective temperature (T_{eff}), surface gravity ($\log g$), and eddy diffusion parameter ($\log K_{zz}$). We compared each provided model against the observed *forcepho* photometry, and varied the overall normalization of the model for a fourth free parameter. The adopted best fit was the one that resulted in the minimum χ^2 for each of our candidates.

We additionally fit the candidates using the ATMO 2020 solar metallicity brown dwarf atmosphere and evolutionary models from Phillips et al. (2020). These were generated using a 1D-2D atmospheric modeling code designed to study hot Jupiters and brown dwarfs, and the ATMO 2020 release includes both atmospheric and evo-

lution models. For simplicity, we adopted the atmospheric chemical equilibrium models with only two free parameters: effective temperature and surface gravity. We performed a similar fit using these models as was done with the Sonora Cholla models, where the best fit was the one corresponding to the minimum χ^2 .

3. RESULTS

3.1. Physical Properties

We present the full list of JADES and CEERS brown dwarf candidates in Table 1, with the *forcepho* fluxes and effective radii. Our naming convention starts with the survey name (JADES or CEERS), the region of the sky (GOODS-S, GOODS-N, or EGS), “BD” indicating brown dwarf candidate, and a unique integer based on the RA of the source. We plot the SEDs for the selected brown dwarf candidates in Figures 2, 3, and 4 and indicate T_{eff} , $\log g$, $\log K_{zz}$, and minimum χ^2 of the best-fitting Sonora Cholla model. In each panel, we also provide the minimum χ^2 derived from the EAZY galaxy fits to the source, the best-fitting photometric redshift, and show the galaxy template fit for each object.

To estimate the distances to the BD candidates based on the fits, we followed the procedure detailed in Wang et al. (2023). The best-fit normalization of the Sonora Cholla models to the observed photometry is equal to $(R/D)^2$, where R is the radius of the model source and D is the distance to the object. We used the “Sonora Bobcat” evolution models (Marley et al. 2021) to find

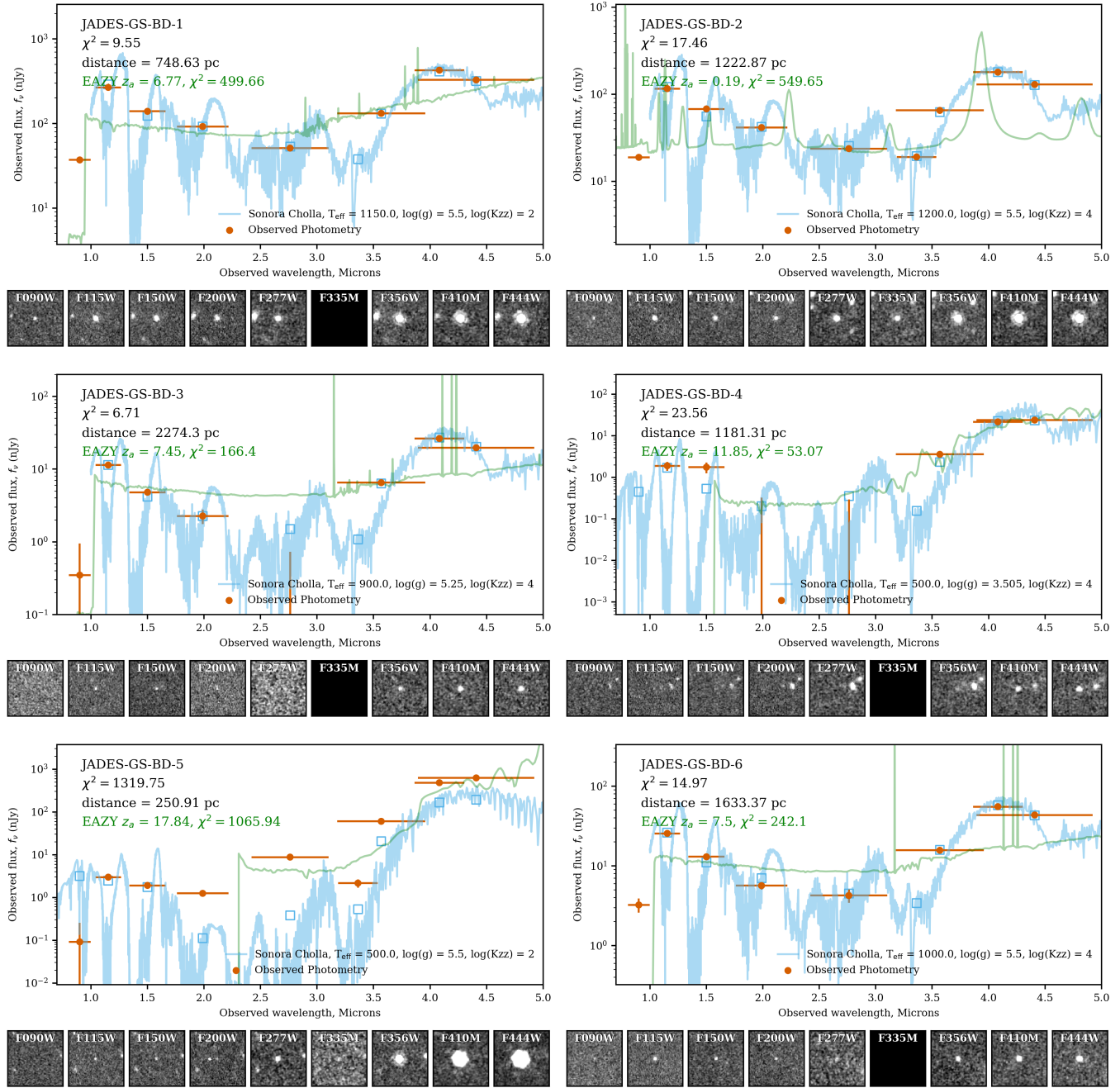


Figure 2. Brown dwarf candidate SEDs measured using *forcepho* (red) with best-fits from the Sonora-Cholla substellar atmospheric models (blue) overlotted. We show the parameters for the model in the bottom right, and the χ^2 of the fit and derived distance based on the model in the upper left. We plot the best-fitting EAZY fit in green, and provide the photometric redshift derived from the fit and the resulting χ^2 . Beneath each SED plot are the individual JWST NIRCcam thumbnails (2'' x 2'') for each source. This is continued in Figure 3 and 4.

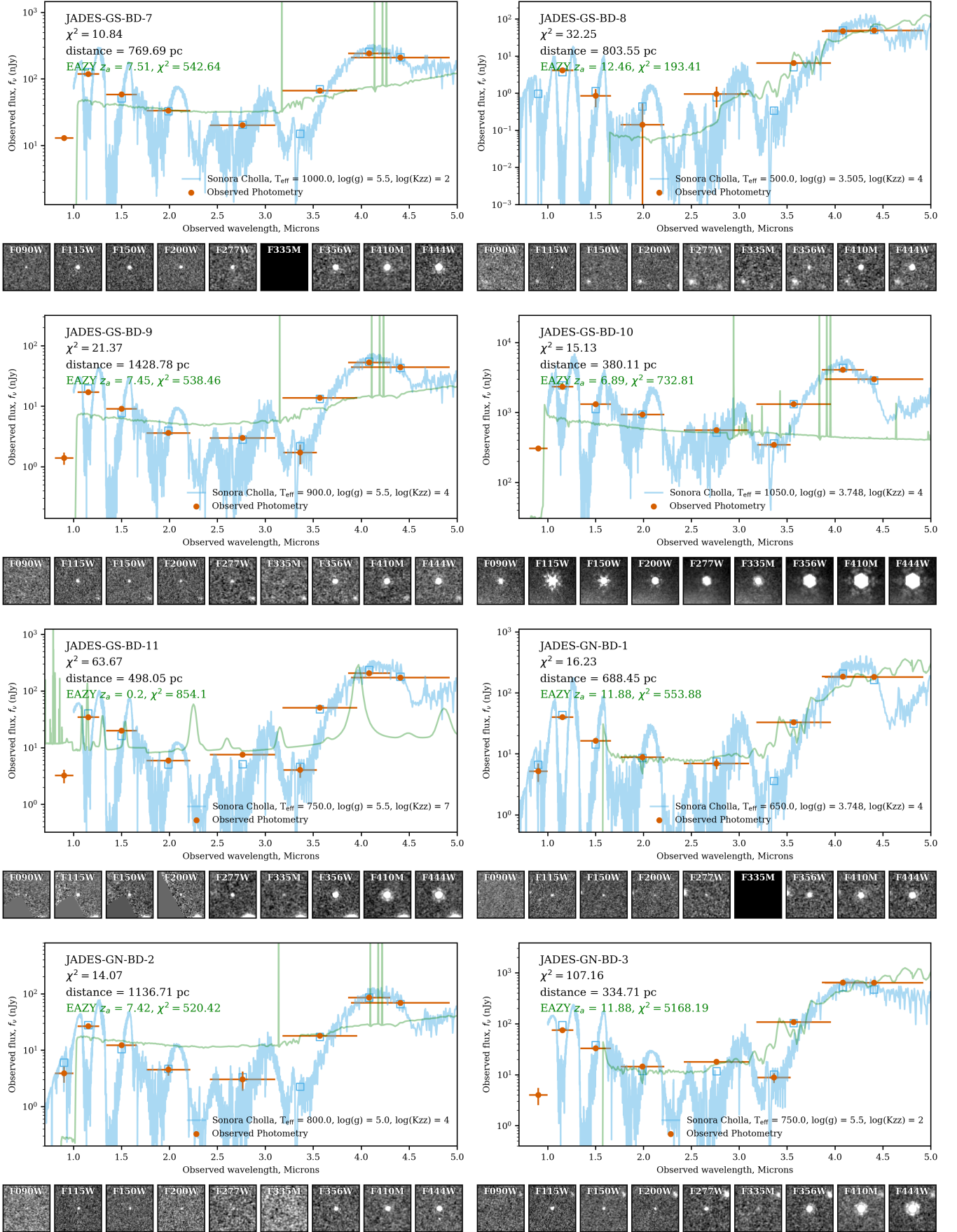


Figure 3. Brown Dwarf Candidate SEDs (continued from Figure 2).

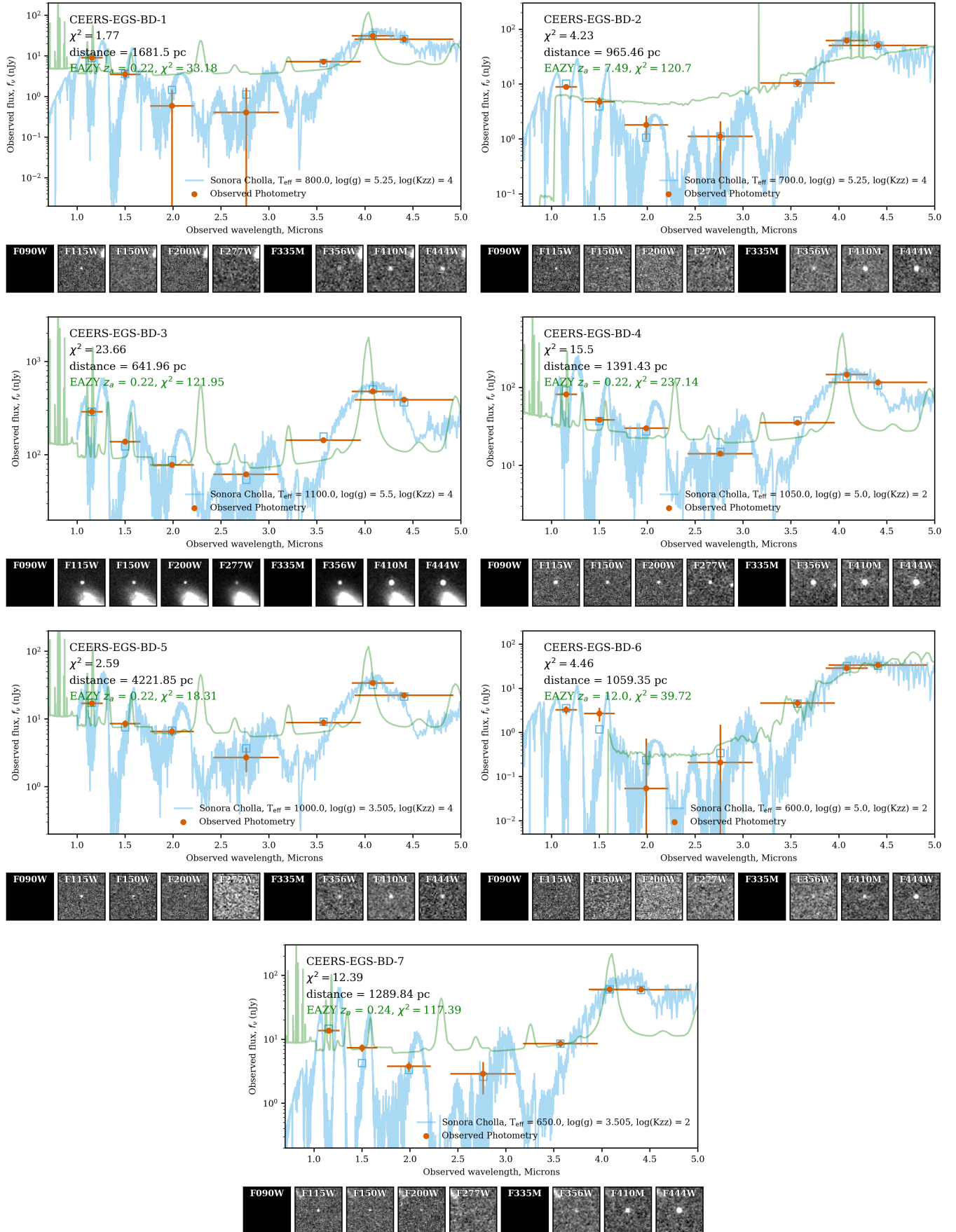


Figure 4. Brown Dwarf Candidate SEDs (continued from Figure 3).

the brown dwarf radii corresponding to the best-fit T_{eff} and $\log g$ values for both solar metallicity ($[M/H] = 0$) and subsolar metallicity ($[M/H] = -0.5$) models. Evolution models use energy loss rate estimates to explore how brown dwarf radii and luminosity change over time. Because the (Marley et al. 2021) Sonora Bobcat evolution models do not include radii for brown dwarfs with $\log g = 5.5$, we extrapolate the models to estimate those values. For the ATMO 2020 fits, we followed the same procedure and estimated the radius of each source from the provided evolutionary models, which allowed us to calculate distances.

As part of the Sonora Bobcat model data release, the authors provide observed photometry at 10 pc for different values of T_{eff} , $\log g$, and radius. To demonstrate the uncertainty in distance estimates to these sources, we additionally fit our candidate photometry directly to the Sonora Bobcat model photometry, and we derive a third distance estimate from the scaling to the observed photometry for our candidates.

In Table 2, we provide the best-fitting parameters, the derived substellar radii, and the distances for our candidates for the Sonora Cholla and ATMO 2020 fits. We also provide the distances and parameters from fitting directly to the Sonora Bobcat model photometry. Using the subsolar Sonora Bobcat models results in distance measurements that are only 0.6% smaller. We do see a more significant difference when comparing to the distances derived directly from the Sonora Bobcat evolutionary models, which are, on average, 11% larger than what we estimate using the Sonora Cholla models. Fits with the ATMO 2020 models result in distances that are 17% larger than those derived using the solar metallicity Sonora Cholla models. At these best-fit effective temperatures, adopting the Sonora Cholla fit values, fourteen of these sources are T dwarf candidates (700K to 1300K), and the remaining seven are Y dwarf candidates (<700K).

In addition, in Table 1, we also provide the measured *forcepho* half-light radii for these candidates. Each of the JADES and CEERS candidates in our sample has a half-light radius less than $0.005''$, which strongly supports the argument that they are unresolved. In addition, the image thumbnails shown in Figures 2, 3, and 4 often have long wavelength morphologies with observable diffraction features, indicating the sources are unresolved.

3.2. Proper Motions

The JADES regions, and portions of the EGS, have been targeted by deep HST/WFC3 observations out to $1.6\mu\text{m}$. These observations, which, in some cases, date

back to 2010, can be used to explore potential proper motion in these sources, which would rule out them being extragalactic in origin. We only detect 8 sources in the WFC3 data, five in GOODS-S, two in GOODS-N, and one in CEERS, and we observe proper motion in only six. We do not observe a proper motion for two sources, JADES-GS-BD-6 or JADES-GN-BD-2.

Using the *photutils* centroids package, we calculated the center of the source in both the HST and the JWST observations independently, and we plot the thumbnails in Figure 5 with circles indicating the recovered centroid positions. In addition, we provide the measured difference in position, which ranges from $0.12''$ for JADES-GS-BD-1 to $0.75''$ for JADES-GN-BD-3. We queried the MAST HST archive through *astroquery* package and obtained the HST WFC3 observation time of these brown dwarf candidates. We found that the mean time difference between the HST and JWST observations were 9–11 years. If we use those mean observed times for the individual sources, we derive proper motions of $0.013''/\text{yr}$ for JADES-GS-BD-1, $0.013''/\text{yr}$ for JADES-GS-BD-7, $0.017''/\text{yr}$ for JADES-GS-BD-10, $0.050''/\text{yr}$ for JADES-GS-BD-11, $0.074''/\text{yr}$ for JADES-GN-BD-3, and $0.022''/\text{yr}$ for CEERS-EGS-BD-3.

We also searched for proper motions by comparing the JADES observations made in late 2022 to more recent medium-band NIRCcam observations of the JADES Origins Field (JOF, PID 3215; Eisenstein et al. 2023b). These data were reduced in a similar manner to that of the JADES data as described in Section 2, including the derivation of an astrometric solution based on Gaia stars. Because of the size of the JOF, we only detected two of our candidates in these observations, JADES-GS-BD-2 and JADES-GS-BD-5. For JADES-GS-BD-2, we don't detect an offset between the NIRCcam F300M position measured from the JOF data and the F277W position measured from the JADES observations. For JADES-GS-BD-5, there is an $0.05''$ difference in the NIRCcam F300M position measured from the JOF data and the F277W position measured from the JADES observations, implying a $0.05''/\text{yr}$ proper motion for the source.

We additionally searched through the Spitzer Space Telescope archive to see if any of our candidate brown dwarfs were detected in observations using IRAC instrument taken as part of the GOODS Spitzer Legacy program (Dickinson et al. 2003). We specifically looked at the images taken in the IRAC2 ($4.5\mu\text{m}$) channel, as, from the SEDs, our candidates are brightest at this wavelength and therefore more likely to be detected. Only two sources were detected, JADES-GN-BD-3 and JADES-GS-BD-5. As JADES-GN-BD-3 is also observed

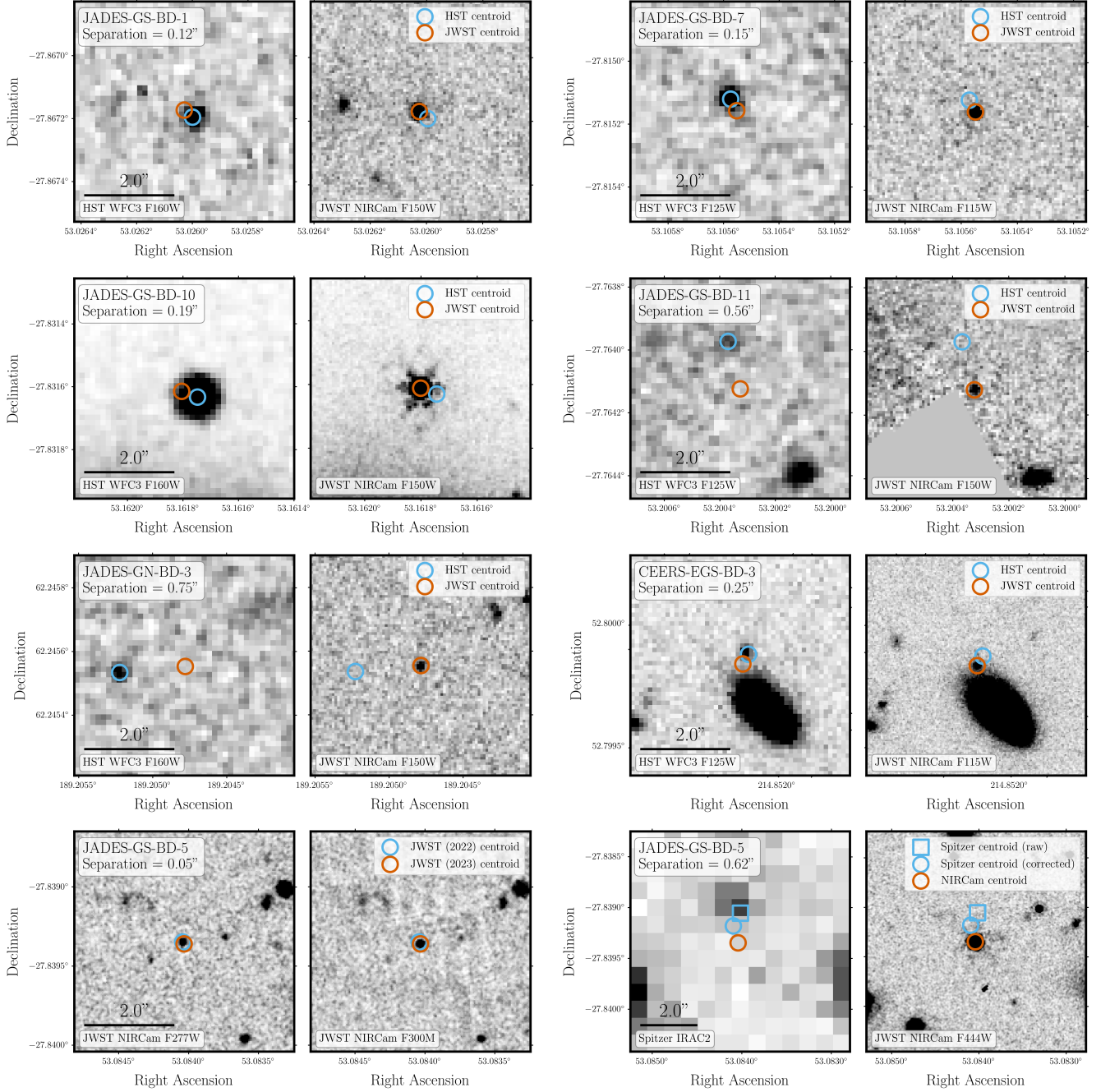


Figure 5. Proper motion measurements between the HST WFC3 and JWST NIRCcam or between two epochs of JWST NIRCcam observations. We plot seven sources, and for each source we plot the first epoch of observations in the left panel, and the second epoch in the right panel, with the filter being used shown in the bottom left. We also plot a scale bar in the left panels, above the filter name. In each panel, the centroid measured for the source from the HST, Spitzer, or JWST observations is shown with a blue circle, and the centroid for the source from the JWST observations is shown in a red circle. The offset, in arcseconds, is provided. For JADES-GS-BD-5, we show two independent measurements of the proper motion. The bottom left pair of panels show an offset between JADES data taken in late 2022 and observations as part of the JADES Origins Field (Eisenstein et al. 2023b) in late 2023. The bottom right pair of panels show a detected offset between Spitzer IRAC2 observations and the JADES F444W observation. Because the Spitzer IRAC2 image has a different WCS than the JADES NIRCcam mosaic, we measure the raw centroid and label it with a square symbol, and the centroid corrected to the JADES WCS is plotted with a circle, along with the corresponding separation.

in the HST WFC3 mosaic, we will use this measured separation for the proper motion measurement owing to the resolution of HST. We should note that the westward direction of the observed motion for JADES-GN-BD-3 is the same between the HST and Spitzer observations.

For JADES-GS-BD-5, this source is too faint at $< 2\mu\text{m}$ to be observed in the WFC3 data. To measure the offset in the Spitzer IRAC2 observation, we used the same method as was used to measure the HST WFC3 offsets, but we had to correct for the fact that the IRAC2 world coordinate solution (WCS) is offset from the Gaia-derived frame used in the JADES mosaics. To estimate this correction, we found the offset for the centroid of a nearby bright star, and subtracted this offset from the measured Spitzer centroid position. In Figure 5, we show JADES-GS-BD-5 with both the measured Spitzer position of the source as well as the corrected position, and derive a difference between the two positions of $0.62''$. Given the positional accuracy of the Spitzer IRAC instrument ($< 0.3''$ as per the Spitzer IRAC Knowledgebase⁴), this is a $> 2\sigma$ offset. The date range provided for this Spitzer observation is August 12 2004 to August 18 2004, which would indicate a proper motion for JADES-GS-BD-5 of $\sim 0.033''/\text{yr}$, which is slightly lower than the value we measured based on the NIRCcam observations, but given the uncertainty in our WCS correction, these values are in agreement. More importantly, the direction of the offset (south, and very slightly to the west), is almost identical between the two independent measurements of the proper motion.

3.3. Discussion of Individual Sources

Because of the number of candidate sources in our sample, below, we will discuss each source individually, highlighting any previous discussion of these objects in the literature. For each source, we present an approximate subdwarf classification based on the best-fit effective temperatures following Burgasser et al. (2002). The true classification requires spectroscopic follow-up of these sources.

3.3.1. JADES-GS-BD-1

This source is very bright, with fluxes above 100 nJy in five of the JADES filters, and the Sonora Cholla fit accurately matches the observed fluxes. The fit indicates that the source is at $T_{\text{eff}} = 1150\text{K}$ (T3-T5), and a distance of ~ 750 pc. This source is unresolved, and has an observed separation between the HST WFC3

F160W image and the JWST NIRCcam F150W image of $0.12''$. Given the HST detection, it is puzzling that this source does not appear to have been written about: a search through the literature for any sources within $5''$ of the WFC3 position of this object did not result in any matches.

3.3.2. JADES-GS-BD-2

This source is a very bright candidate (F410M flux of ~ 180 nJy) detected significantly at all of the JADES NIRCcam wavelengths, with obvious diffraction features in the 3 - $4\mu\text{m}$ images, suggesting that it is unresolved. The larger χ^2 of the Sonora Cholla fit is due in large part to the mismatch in the F150W filter, while the resulting fit does accurately match the observed fluxes, indicating that this is potentially an early T dwarf at 1.2 kpc. The EAZY galaxy template fit does not accurately predict the relatively fainter F277W and F335M fluxes in this source, attributing the LW emission to $3.3\mu\text{m}$ PAH emission.

3.3.3. JADES-GS-BD-3

This brown dwarf candidate has an excellent Sonora Cholla fit with $T_{\text{eff}} = 900\text{K}$ (T5-T6) and a derived distance of 2.2 kpc. The Sonora Bobcat fit has a slightly higher temperature (1000 K), and results in a distance of almost 3.5 kpc, which would place it firmly in the Milky Way halo. The extremely blue F115W - F200W color and the lack of an F277W detection make it difficult to conclude that the source is extragalactic.

3.3.4. JADES-GS-BD-4

This brown dwarf candidate is very faint at wavelengths shorter than $3.5\mu\text{m}$, with fluxes of only ~ 2 nJy in F115W and F150W, and no significant detections in F200W or F277W. The Sonora Cholla fit for this source indicates that it is only a 500 K (Y dwarf) source at a distance of almost 1.2 kpc, and this is one of three sources where the Sonora Cholla fit results in such a low temperature. The EAZY redshift ($z_a = 11.85$) is ruled out due to the detection of F115W flux shortward of the best-fit Lyman break. In the absence of detections at short wavelengths, this source would appear to be a dusty red galaxy or even an F277W dropout at $z > 20$. Faint Y-dwarfs should be explored as possible alternate explanations for ultra high-redshift JWST galaxy candidates.

3.3.5. JADES-GS-BD-5

This brown dwarf candidate has a Sonora Cholla fit with $\chi^2 = 1320$, but this is driven by the small uncertainties on the fluxes, the blue F277W - F335M color in

⁴ https://irsa.ipac.caltech.edu/docs/knowledgebase/spitzer_irac.html

Table 2. Derived Properties of the Brown Dwarf Candidates

Object ID	Sonora Cholla					Sonora Bobcat				ATMO 2020			
	T_{eff} (K)	$\log(g)$	$\log(K_{\text{zz}})$	$R (R_{\odot})$	D (pc)	T_{eff} (K)	$\log(g)$	$R (R_{\odot})$	D (pc)	T_{eff} (K)	$\log(g)$	$R (R_{\odot})$	D (pc)
JADES-GS-BD-1	1150	5.5	2	0.077	749	1100	5.25	0.086	820	1100	5.5	0.125	1162
JADES-GS-BD-2	1200	5.5	4	0.078	1223	1200	5.25	0.087	1460	1200	5.5	0.079	1295
JADES-GS-BD-3	900	5.25	4	0.085	2274	1000	5.0	0.094	3480	900	5.5	0.078	2351
JADES-GS-BD-4	500	3.505	4	0.128	1181	525	5.25	0.081	1230	500	5.5	0.101	1364
JADES-GS-BD-5	500	5.5	2	0.073	251	375	4.0	0.114	190	350	5.0	0.104	160
JADES-GS-BD-6	1000	5.5	4	0.076	1633	1000	5.0	0.094	2290	900	5.5	0.078	1549
JADES-GS-BD-7	1000	5.5	2	0.076	770	1000	5.5	0.077	880	1000	5.5	0.13	1467
JADES-GS-BD-8	500	3.505	4	0.128	804	500	5.0	0.089	840	500	5.5	0.101	949
JADES-GS-BD-9	900	5.5	4	0.076	1429	900	5.0	0.093	2080	800	5.5	0.097	1710
JADES-GS-BD-10	1050	3.748	4	0.141	380	1100	5.25	0.086	260	1100	5.5	0.125	377
JADES-GS-BD-11	750	5.5	7	0.075	498	750	5.25	0.083	770	700	5.5	0.085	668
JADES-GN-BD-1	650	3.748	4	0.129	688	700	5.0	0.091	740	700	5.5	0.085	696
JADES-GN-BD-2	800	5.0	4	0.093	1137	850	5.5	0.076	1250	800	5.5	0.097	1407
JADES-GN-BD-3	750	5.5	2	0.075	335	600	5.25	0.082	290	600	5.5	0.1	354
CEERS-EGS-BD-1	800	5.25	4	0.084	1682	850	5.25	0.084	2330	800	5.5	0.097	2353
CEERS-EGS-BD-2	700	5.25	4	0.083	965	650	5.5	0.074	1020	600	5.5	0.1	1149
CEERS-EGS-BD-3	1100	5.5	4	0.077	642	1100	5.0	0.095	870	1000	5.5	0.13	984
CEERS-EGS-BD-4	1050	5.0	2	0.095	1391	1000	5.0	0.095	1350	1000	5.0	0.13	1813
CEERS-EGS-BD-5	1000	3.505	4	0.145	4222	1100	5.25	0.086	3100	1100	5.5	0.125	4503
CEERS-EGS-BD-6	600	5.0	2	0.09	1059	525	5.0	0.09	1130	500	5.0	0.101	1098
CEERS-EGS-BD-7	650	3.505	2	0.133	1290	650	5.0	0.09	1080	600	4.5	0.1	1006

this source (it is the only object in our sample not selected by the F115W-F277W-F444W criteria shown in the middle panel of Figure 1), and the relative lack of flux at $< 1.6\mu\text{m}$. The best-fit results in a low effective temperature (500 K, a Y dwarf) and positions the source at only 251 pc away, the closest among the entire sample. As discussed earlier in this section, this source has an observed proper motion between the Spitzer IRAC2 and JWST NIRCcam F444W observations of $0.62''$ after correcting for the different reference frames. This best galaxy template EAZY fit returns a photometric redshift of $z_a = 17.84$, which is at odds with the observed F115W, F150W, and F200W fluxes, and the χ^2 is still significantly worse than the Sonora Cholla fit. This could result from a limitation of the cloud-free Sonora Cholla models, as any clouds, or differences in the molecular absorption from the models, would significantly change the shape of the SED. While the source could be a binary brown dwarf system (see Burgasser et al. 2003a; Cruz et al. 2004; Burgasser et al. 2006; Dupuy et al. 2015; Kiwy et al. 2022; Calissendorff et al. 2023, for examples in the literature), this may not significantly effect the observed colors.

3.3.6. JADES-GS-BD-6

This source is quite well fit by a 1000 K Sonora Cholla model, indicating that it is potentially a T5-T6 dwarf at a distance of 1.6 kpc. The EAZY galaxy template attempts to replicate the very blue F115W - F277W color with a Lyman break and the red F356W - F444W color with [OIII] λ 5007 emission boosting the F410M and F444W fluxes, but the resulting fit is very poor.

3.3.7. JADES-GS-BD-7

The Sonora Cholla fit for this candidate indicates that it is at 1000K (T5 - T6), at a distance of ~ 800 pc. The fit is significantly better than the lowest χ^2 EAZY fit, and the evidence for this source being within the Milky Way is strengthened by the $0.15''$ separation between the HST WFC3 F125W centroid and the JWST NIRCcam F115W centroid. This source was discussed previously in Oesch et al. (2012), Lorenzoni et al. (2013), and Finkelstein et al. (2015). Oesch et al. (2012) removed the source from their list of $z \sim 7$ candidates as it had colors consistent with being a T-dwarf. It should be noted that the proper motion between the HST and JWST observations for this source was first discussed in Bunker et al. (2023) under the ID 10035328.

3.3.8. JADES-GS-BD-8

This source is at $\text{SNR} > 10$ in the F115W, F356W, F410M and F444W filters, but has $\text{SNR} < 3$ in the other

JADES NIRCcam filters. The best Sonora Cholla fit indicates the source could possibly be a 500K Y-dwarf at 804 pc, while the best EAZY fit indicates the source could be at $z = 12.46$, a redshift ruled out by the F115W detection. The coverage at $1.15 \mu\text{m}$ is very important for helping to confirm these faint Y-dwarfs.

3.3.9. JADES-GS-BD-9

This source is bright, with a point-like morphology and an excellent Sonora Cholla fit with $T_{\text{eff}} = 900\text{K}$ (T6 - T7) indicating a distance of 1.4 kpc. The poor EAZY fit significantly overpredicts the $1.5 - 3.5\mu\text{m}$ flux for this source.

3.3.10. JADES-GS-BD-10

This candidate is the brightest source in our sample, with an F410M flux of > 4000 nJy. The Sonora Cholla fit agrees with the observed photometry quite well, and indicates that the source is potentially at 1050 K (T0 - T3), at a distance of 380 pc. The EAZY fit is much worse, and while a $z_a = 6.89$ galaxy solution is possible, it overpredicts the F277W and F335M fluxes. This source has a proper motion of $0.017''/\text{yr}$, and so an extragalactic origin is unlikely. It has been very well studied in the literature owing to its brightness, and was first discovered in a search for $z \sim 6$ galaxies in GOODS-S in Stanway et al. (2003), where the authors suggest it is likely a star owing to its colors. Later, in Vanzella et al. (2009), the authors remove the source from a list of high-redshift candidate galaxies due to detection of proper motion.

3.3.11. JADES-GS-BD-11

This brown dwarf candidate is near a gap in the short-wavelength JADES mosaic, as seen in the thumbnails in Figure 3. The `forcepho` flux measurements were not affected by the position of the source, and this source is quite bright (~ 200 nJy at $4\mu\text{m}$). The best Sonora Cholla fit returns $T_{\text{eff}} = 750\text{K}$ (T9) at ~ 500 pc. This source has an observed offset of $0.56''$ between the HST WFC3 F125W and JWST NIRCcam F150W positions. In addition, this source is GSDZ-2480745501 in Bouwens et al. (2015), with an $z_{\text{EAZY}} = 6.69$, which would put the Lyman break at $0.93\mu\text{m}$. The very red LW color (F335M - F444W = 4.07), and the observed proper motion call this interpretation into doubt.

3.3.12. JADES-GN-BD-1

This candidate is very faint at short wavelengths, and both bright and unresolved at longer wavelengths, with fluxes of around almost 200 nJy at F410M and F444W. The best fit from the Sonora Cholla models suggests that the candidate is only at 650 K (an early Y dwarf) at only ~ 700 pc away. The EAZY galaxy template fit

is very poor, with a photometric redshift of 11.88 in disagreement with the significant F115W detection.

3.3.13. JADES-GN-BD-2

The Sonora Cholla best fit for this source is an 800K (T7 - T8 dwarf) model at 1 kpc, the furthest observed in GOODS-N. The EAZY fit, which cannot account for the observed faint F200W, F277W, or F335M emission, attempts to fit the source as an F090W dropout with strong line emission, and has a significantly worse χ^2 .

3.3.14. JADES-GN-BD-3

This brown dwarf candidate in GOODS-N is detected in each of the JADES NIRCcam bands, with ~ 700 nJy fluxes in F410M and F444W. As a result, the uncertainties on the fluxes are quite small, leading to a large χ^2 for the Sonora Cholla fit. However, from Figure 2, it can be seen that the fit accurately matches the fluxes and the resulting parameters suggest that the source could be nearby (334 pc) with $T_{\text{eff}} = 750$ K (Y dwarf). This source has a proper motion of $0.074''/\text{yr}$, the largest we observe in our sample. This lends strong credibility to this source being within our own Galaxy.

A source at the HST location of this object was discussed in Bouwens et al. (2015) and Finkelstein et al. (2015) as a $z \sim 7$ galaxy, likely due to the HST WFC3 observations only probing out to $1.6\mu\text{m}$. An analysis by Endsley et al. (2021) of the Spitzer observations for this source noted its red $3.6 - 4.5 \mu\text{m}$ color, but it was not included in their final sample of $z \sim 7$ [OIII]+H β emitters.

3.3.15. CEERS-EGS-BD-1

The Sonora Cholla model for this source has a best-fit $T_{\text{eff}} = 800$ K (T7 - T8) at a distance of 1.7 kpc. The fit is significantly better than the EAZY fit, which overpredicts both the F200W and F277W non-detections and the F814W flux.

3.3.16. CEERS-EGS-BD-2

The brown dwarf candidate has an excellent fit ($\chi^2 = 4$) with $T_{\text{eff}} = 700$ K (T8 - L0) and a distance of 970 pc.

3.3.17. CEERS-EGS-BD-3

This candidate is the brightest among the CEERS sources, with F410M flux of ~ 480 nJy. It is located north of a galaxy (separated by $1.4''$) at $z_{\text{spec}} = 0.82$ (Momcheva et al. 2016). The Sonora Cholla fit indicates that the object could be at $T_{\text{eff}} = 1100$ K (T2 - T5) and a distance of 642 pc. We also observe a proper motion of $0.022''/\text{yr}$ for the source, demonstrating that this source is likely not extragalactic in nature. A search

through the literature for sources detected at this HST-derived position did not return any matches, potentially due to the proximity to the nearby galaxy.

3.3.18. CEERS-EGS-BD-4

This brown dwarf candidate is the brightest across the CEERS footprint, with an F444W flux of 116 nJy, and the Sonora Cholla fit is significantly better than the EAZY fit ($\chi^2 = 237$). The best fit indicates a $T_{\text{eff}} = 1050$ K (T3 - T5), with a distance of 1.4 kpc. In this source, and multiple other CEERS sources, the EAZY fit predicts a flux at $< 1\mu\text{m}$ that is not observed in the HST ACS F814W mosaics.

3.3.19. CEERS-EGS-BD-5

This Sonora Cholla fit to this source has a $\chi^2 = 2.7$, $T_{\text{eff}} = 1000$ K (T4 - T6), and most importantly, a predicted distance of 4.2 kpc, making it the farthest brown dwarf candidate in our sample. The EAZY fit to the NIR-Cam data predicts an F814W detection that we do not observe (the $0.2''$ diameter circular aperture flux for this source is -0.3 ± 1.8 nJy, consistent with zero). If this source were a galaxy, it would need to have a strong hot dust component coupled with a very blue UV slope ($\beta = -3.75_{0.28}^{0.25}$). At this slope, it would be a significant outlier among the JADES sample of F090W dropout galaxies assembled by Topping et al. (2023).

3.3.20. CEERS-EGS-BD-6

This source is not significantly detected in F200W or F277W, and is only detected at $\text{SNR} = 5.1$ in F115W and $\text{SNR} = 2.9$ in F150W. The best-fit indicate a $T_{\text{eff}} = 600$ K (Y dwarf) at 1.1 kpc. The EAZY fit, at $z_a = 12.0$, is not in agreement with the observed F115W flux.

3.3.21. CEERS-EGS-BD-7

The best-fit parameters for the Sonora Cholla fit to the photometry for this source indicate a $T_{\text{eff}} = 650\text{K}$ (late T or early Y dwarf) at 1.3 kpc. The fit, however, underpredicts the observed F150W, F200W, and F277W fluxes.

4. DISCUSSION

In this section, we will discuss the implications of these brown dwarf candidates by exploring their positions within the Milky Way and distances from the Sun, as well as their observed colors with an eye towards how these types of objects can be detected in current and future deep extragalactic catalogs.

4.1. Position in the Milky Way

In Figure 6, we plot the positions of our brown dwarf candidates with respect to the Sun and our Galaxy. For

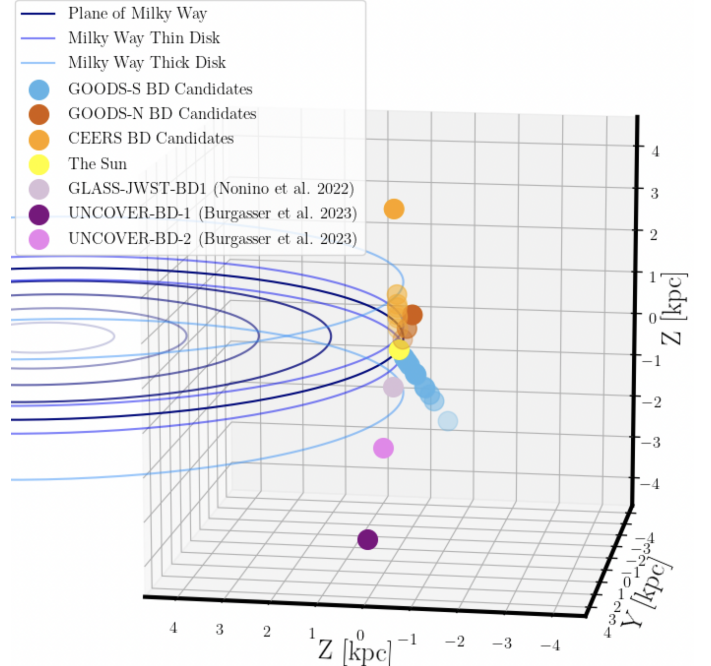


Figure 6. Positions of the JADES and CEERS brown dwarf candidates, with JADES GOODS-S sources in shades of blue, JADES GOODS-N sources in shades of red, and CEERS sources in shades of orange, plotted in three dimensional space with respect to the Milky Way Galaxy disk. The darker the shade, the closer the source is to the viewpoint of the plot. The distances for these sources are from fits using the Sonora Cholla models along with the solar metallicity Sonora Bobcat models. We show the central plane of the Milky Way with a navy blue line, and then the thin and thick disk with lighter blue lines. We also plot the Sun as a yellow circle, and the spectroscopically-confirmed brown dwarfs from the UNCOVER and GLASS surveys (Nonino et al. 2023; Langeroodi et al. 2023; Burgasser et al. 2023) with purple points. For these sources, we adopt the distances derived in Burgasser et al. (2023).

this figure, we adopt the distances measured using the Sonora Cholla models using the solar metallicity Sonora Bobcat evolutionary models given in Table 2. We plot the GOODS-S sources with blue points, the GOODS-N sources with red points, and the CEERS sources with orange points. We include the Nonino et al. (2023) GLASS brown dwarf, as well as the two UNCOVER brown dwarfs discussed in Langeroodi et al. (2023) and Burgasser et al. (2023), with purple points. For these three sources, their distances are taken from Burgasser et al. (2023). We also plot the plane of the Milky Way with blue curves. The darkest blue curve represents the central plane of the Galaxy, with the thin disk (300 pc scale height) and thick disk (1.4 kpc scale height) represented with lighter blue curves. The bulk of the JADES candidates lie within the thick disk, although there are

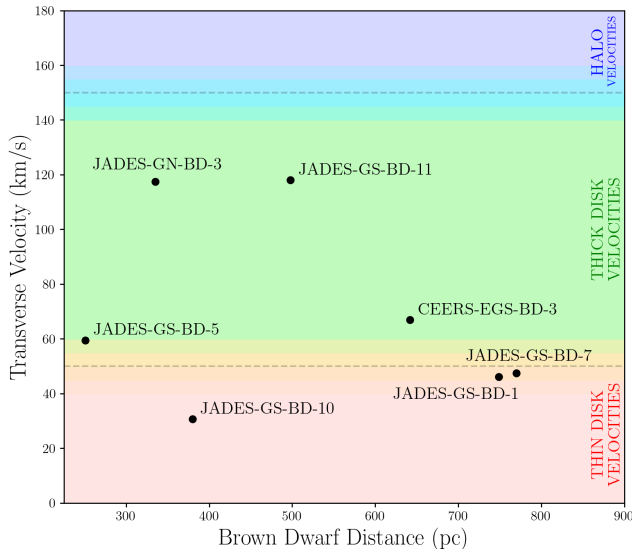


Figure 7. Transverse velocities of the brown dwarf candidates plotted against their estimated distances. We also show, with colored bands and dashed lines, the approximate transverse velocity ranges of observed thin-disk objects (0 - 50 km/s), thick-disk objects (50 - 150 km/s), and halo objects (> 150 km/s). The bulk of the brown dwarf candidates with proper motions in our sample have transverse velocities similar to thick-disk objects.

four that may be outside the thick disk in the Galactic halo (JADES-GS-BD-6, JADES-GS-BD-3, CEERS-EGS-BD-5, and CEERS-EGS-BD-1). It should be cautioned that the distance estimates from the fitting are highly uncertain.

To better explore the nature of these brown dwarf candidates, we calculated their transverse velocities from their proper motions and distances using the equation $v_T = 4.74\mu d$ (here, v_T is the transverse velocity in km/s, μ is the proper motion in arcseconds per year, and d is the distance in parsecs). We estimate transverse velocities with respect to the Sun of 46 km/s for JADES-GS-BD-1, 59 km/s for JADES-GS-BD-5, 47 km/s for JADES-GS-BD-7, 31 km/s for JADES-GS-BD-10, 118 km/s for JADES-GS-BD-11, 118 km/s for JADES-GN-BD-3, and 67 km/s for CEERS-EGS-BD-3. These values are, on average, higher than more local brown dwarfs at similar temperatures from Kirkpatrick et al. (2021), where most have transverse velocities below 50 km/s. We plot these values against our estimated distances in Figure 7. On this Figure, we indicate ranges in transverse velocity corresponding to the thin disk (0 km/s - 50 km/s), thick disk (50 km/s - 150 km/s) and halo (> 150 km/s) populations with colored bands (Casertano et al. 1990; Robin et al. 2003; Nissen 2004). While the transverse velocities for the sources in our sample

with proper motion agree with those in the thin and thick disks, their distances in combination with these velocities provide strong evidence that these sources are members of the thick disk of the Galaxy.

Several authors have explored the number density of low-mass stars and brown dwarfs in the Milky Way from both observations and simulations. Ryan & Reid (2016) provided predicted number densities for ultra-cool dwarfs between spectral types M8-T8 for thin and thick disk exponential models motivated by estimates of their luminosity function. These authors predict a number density of T0-T5 dwarfs at all observed magnitudes (combining the thick and thin disk estimates) in GOODS-S of $3.43 \times 10^{-2} \text{ arcmin}^{-1}$, in GOODS-N of $3.32 \times 10^{-2} \text{ arcmin}^{-1}$, and in the EGS of $3.84 \times 10^{-2} \text{ arcmin}^{-1}$. Given the current JADES area of 67 arcmin^2 for GOODS-S, 58 arcmin^2 for GOODS-N, and 90.8 arcmin^2 in the CEERS area in the EGS, the Ryan & Reid (2016) prediction would be 2.3 T-dwarfs across the JADES GOODS-S footprint, 1.9 across GOODS-N, and 3.5 across CEERS. If we define the T0 - T5 dwarf temperature range as $T_{\text{eff}} \sim 1000 - 1300\text{K}$ (Burgasser et al. 2002), then we find only five candidates in GOODS-S with best fits in this temperature range, none in GOODS-N, and 3 in the CEERS EGS footprint. This is in statistical agreement with the combined prediction across GOODS-S, GOODS-N, and CEERS EGS from Ryan & Reid (2016).

An alternate method of comparing the observed number density of brown dwarf candidates is adopted by Wang et al. (2023), where these authors compare the likelihood of finding their source, CEERS-BD1, with the the observed space density of early-L through early-Y dwarfs from Kirkpatrick et al. (2021). Table 15 in Kirkpatrick et al. (2021) provides space densities as a function of T_{eff} complete only out to 20 pc. If we co-add the number densities of T0 to Y1.5 sources from this table, these authors estimate a total of $14.92 \times 10^{-3} \text{ arcmin}^{-1}$. which, If we multiply this estimate by the total area of the JADES GOODS-S and GOODS-N and CEERS EGS footprints (216 arcmin^2), implies only 3.2 brown dwarfs across this entire temperature range. The bulk of the candidates in our sample have best-fit distances outside the thin disk probed by the Kirkpatrick et al. (2021) sample, however. Indeed, these results and others in the literature can be added to the growing number of substellar candidates found in extragalactic deep fields as discussed in the Introduction.

4.2. Comparing to High-Redshift Galaxy Colors

As discussed in Section 3, some of the brown dwarf candidates in our sample have previously appeared in

the literature as potential high-redshift galaxies owing to them being selected as dropout galaxies at $0.9\mu\text{m}$ and the limited HST WFC3 wavelength coverage in the near-IR. Following work exploring the use of the 3 - $4\mu\text{m}$ slope in separating brown dwarf candidates from F090W dropouts in Hainline et al. (2020), in Figure 8 we plot the F090W - F115W colors vs. the F335M - F444W colors for the JADES survey objects with $m_{F444W} < 28.5$. Because the CEERS survey does not include coverage in F090W or F335M, we do not plot any CEERS sources. We also plot the six brown dwarf candidates in our sample with detections in F090W, F115W, F335M, and F444W. As a subsample of the high-temperature Sonora Cholla models do not extend to wavelengths that cover the entirety of the F090W filter, we instead include the predictions from ATMO 2020, with points colored by the effective temperature of the model. The F335M fluxes are quite low in our candidates, which, if these were brown dwarfs, would be caused by molecular absorption by CH_4 at 3 - $3.6\mu\text{m}$.

We additionally plot a sample of $z = 8.0 - 8.5$ galaxy candidates from Hainline et al. (2023). In this redshift range, these sources are F090W Lyman dropouts. Similar to the high- z sample, we measure $F090W - F115W > 1$ for the brown dwarf candidates (five of the six have $F090W - F115W > 2$). The low-temperature brown dwarf candidates differentiate themselves from the high- z sample by having $F335M - F444W > 2.0$. While ionized emission (e.g. $[\text{OIII}]\lambda 5007$) can provide extra flux in the F410M and F444W filters, there are no galaxies in the $z = 8.0 - 8.5$ JADES sample with $F335M - F444W$ colors similar to that of the low-mass brown dwarfs. At higher temperatures, the predicted ATMO 2020 colors for late M and early Y dwarfs are similar to the F090W dropouts, however.

In Labbe et al. (2023), the authors selected sources red LW colors from the JWST Ultradeep NIRSpec and NIRCам Observations before the Epoch of Reionization survey (Bezanson et al. 2022, UNCOVER). A number of the members of their sample have colors similar to the brown dwarf candidates selected here. The authors fit these sources with both galaxy stellar light as well as reprocessed light from dust heated by accretion onto a supermassive black hole. While these fits can account for the red $F335M - F444W$ colors in these sources, they have difficulties fitting the extremely blue $F115W - F277W$ colors at the same time. The alternate explanation, that a subsample of their sources are unresolved brown dwarf candidates, was recently confirmed by independent reductions of spectroscopy for two of their sources in Langeroodi et al. (2023) and Burgasser et al. (2023). Multiple authors have looked at similar samples

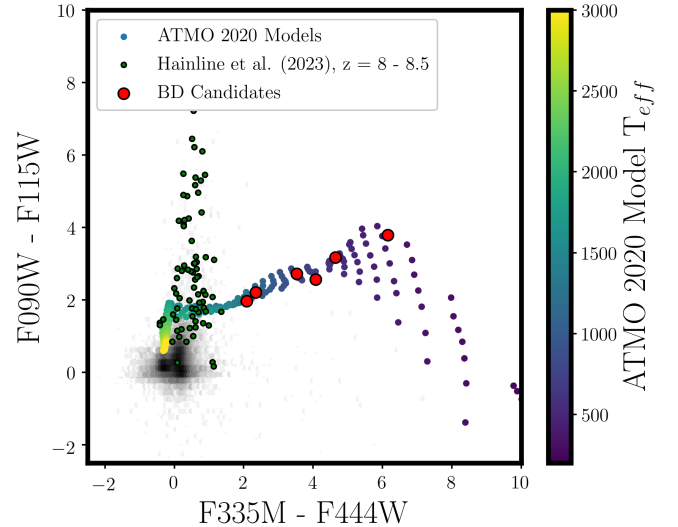


Figure 8. F090W-F115W vs F335M-F444W color. In this plot, we show those JADES sources with $m_{F444W} < 28.5$ in grey, but we plot the brown dwarf candidates detected in F090W, F115W, F335M, and F444W with red circles, as well as the ATMO 2020 model colors with points signifying their effective temperature as shown in the colorbar. In addition, we also plot a sample of F090W Lyman dropout galaxies from Hainline et al. (2023) with EAZY photometric redshifts between $z = 8 - 8.5$. A red $F335M - F444W$ color is helpful for distinguishing between F090W dropout galaxies at $z \sim 8$ and low-temperature brown dwarfs, although at higher temperatures, the ATMO models predict that late M and early L dwarfs would have similar colors to the dropout galaxies.

of extremely red sources in extragalactic datasets (e.g. Barro et al. 2023; Pérez-González et al. 2023; Franco et al. 2023, among others), and we have outlined color selection criteria here which may be used to find the brown dwarfs from among those samples.

If we assume that the candidates in our sample are F090W dropouts at $z = 8.0 - 8.5$, we can measure a potential UV slope for the sources by performing a linear fitting to the F115W, F150W, and F200W fluxes. The resulting slopes, which range between $\beta = -3.62$ (JADES-GS-BD-5) and $\beta = -6.75$ (JADES-GS-BD-8), have a median $\beta = -4.81$. This is significantly bluer than the assembled F090W dropouts selected across the JADES survey in Topping et al. (2023), which have a median $\beta = -2.32^{+0.03}_{-0.02}$. This provides more evidence that these sources are not extragalactic in origin.

4.3. Brown Dwarf Selection in Other Extragalactic Programs

The JADES depth and filter selection, along with the large number of candidate brown dwarfs in our sample, allows us to predict number counts of sources found

in current and future extragalactic JWST programs. In particular, we can compare our sources to the survey depths for the COSMOS-Web (Casey et al. 2022) and PRIMER (Dunlop et al. 2021) programs which will feature NIRCcam photometric coverage across large areas. For COSMOS-Web, the total area will be 1929 square arcmin with 5σ point-source depths of 26.9 - 28.3 across four NIRCcam filters (F115W, F150W, F277W, and F444W). PRIMER will survey 378 square arcminutes with eight filters (F090W, F115W, F150W, F200W, F277W, F356W, F410M, and F444W) down to 5σ point-source depths of 27.6 - 29.5. Because of these extended areas, these surveys should uncover large numbers of these relatively rare brown dwarf candidates similar to those discussed in this paper.

In Figure 9, we plot the SEDs for our sources and indicate the 5σ point-source depths for both the PRIMER and COSMOS-Web filters to demonstrate which of the sources in our sample would be found in these surveys. For COSMOS-Web, we use the values estimated for the deepest portion (4 exposures) of the full survey as measured using $0.15''$ radius apertures and provided in Casey et al. (2022). For PRIMER, we use the measurements for the current data using $0.16''$ radius apertures and provided in Morishita et al. (2023), but we note that this is shallower than the future depths for the completed survey.

Because of how our sources were chosen with $m_{F444W} < 28.5$, each of the sources would be significantly detected in that filter for both PRIMER and COSMOS-Web. However, for the majority of our sources, they are not bright enough at short wavelengths to be observed in these shallow, large area surveys, so the actual selection of these sources would be difficult. When we compare to the COSMOS-Web depths and filters, we do find that six of the sources in our sample have F115W, F150W, and F277W fluxes brighter than the 5σ flux limits, and five of these sources have best-fit $T_{\text{eff}} > 1000\text{K}$. The remaining object, JADES-GN-BD-3, has $T_{\text{eff}} = 750\text{K}$, demonstrating that bright sources with these low effective temperatures, while rare, are still accessible to this survey. We highlight these sources with thick outlined points in Figure 9. One additional source, CEERS-EGS-BD-4, is just fainter than the F277W flux limit for COMOS-Web. Across the JADES+CEERS footprints we find only 2.7×10^{-2} sources arcmin $^{-2}$, which which would result in a total of 52 brown dwarfs bright enough to be detected in all four filters across the COSMOS-Web survey footprint, although this is a rough estimate given the limited number of sources we find. For the current depths of the PRIMER survey the number of sources that satisfy the detection thresh-

old in F115W, F150W, and F277W from our sample is only four, although two additional sources would be detected in F115W and F150W, but not F277W. For the PRIMER depths, then, our sample predicts 1.8×10^{-2} sources arcmin $^{-2}$, and a total of 6.8 brown dwarfs bright enough to be detected in F115W, F150W, F277W, and F444W, although this is at the current depths, which will increase with future observations.

While all of our sources will still be found at $4\mu\text{m}$ at the COSMOS-Web and PRIMER survey depths, to characterize the SEDs of the cooler Y-dwarfs requires deeper observational data targeting primarily the 1 - $2\mu\text{m}$ wavelength range. With such large areas probed, the COSMOS-Web and PRIMER surveys still represent an incredible opportunity for understanding statistical samples of low-mass T-dwarfs and rare bright Y-dwarfs at hundreds of parsec or even kiloparsec distances.

5. CONCLUSIONS

We have searched the first year of deep NIRCcam JADES and CEERS extragalactic photometric data to hunt for low-mass brown dwarf candidates. These sources are vital for understanding the low-mass end of the initial mass function, especially for the types of low-metallicity stars that are found in the Milky Way thick disk and halo. Our primary conclusions are:

1. Using color selection and visual inspection, we found a sample of 21 sources across the combined 215.8 square arcminutes (0.09 candidates arcmin $^{-2}$). These sources were chosen by targeting the blue F115W - F277W and red F277W - F444W colors observed in late L, T, and Y sub-dwarfs.
2. After fitting these sources to the Karalidi et al. (2021) Sonora Cholla models, we find that these objects range in temperature between $T_{\text{eff}} = 500 - 1200\text{K}$, and are at distances of $0.1 - 4.2$ kpc. While the majority of the sources are in the thick disk, we do find four sources that are potentially in the Milky Way halo, based on their distances. These sources are poorly fit with galaxy template models. We find similar results when fitting with the Phillips et al. (2020) ATMO 2020 models, albeit at larger distances.
3. By comparing these sources to existing HST/WFC3 and Spitzer infrared data, we estimate proper motions for seven of the candidates of $0.013''/\text{yr} - 0.074''/\text{yr}$, providing evidence that these sources are not extragalactic in nature. The directions of these proper motions are roughly in line with the axis of the Milky Way.

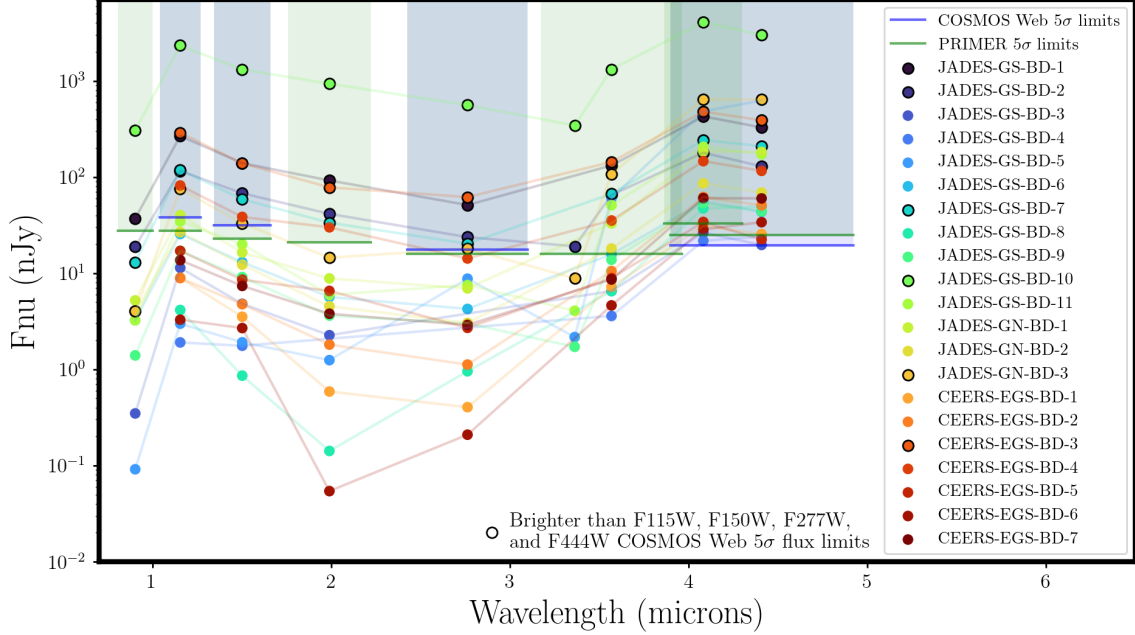


Figure 9. Brown dwarf candidate SEDs plotted along with the 5σ point source depths for the COSMOS Web (blue shaded area) and Primer (green shaded area) surveys. We highlight those sources that would be detected above the COSMOS Web limits in F115W, F150W, F277W, and F444W with black heavy circles. While our sources are bright enough to be detected in F444W and F410M (for PRIMER), at $< 3\mu\text{m}$ the majority are too faint, making characterizing their properties difficult in these large area programs.

4. We present a set of color criteria which can help separate these brown dwarf candidates from NIR-Cam F090W dropouts at $z \sim 8 - 8.5$, which do not have the very red F335M - F444W colors seen in subdwarfs.
5. We use our sample to explore the temperatures of brown dwarfs that might be observed in the PRIMER and COSMOS Web surveys, which probe much larger areas than JADES and CEERS at shallower depths. Based on comparing to the fluxes of our brown dwarf candidates, we find that sources at $T_{\text{eff}} < 1000\text{K}$ are too faint at $< 3\mu\text{m}$ to be seen in these surveys, and will appear only in the F410M and F444W filters. Based on the fluxes of our candidates, we would expect ~ 50 sources across the COSMOS Web survey area bright enough to be detected across all four observational filters.

These sources provide an exciting opportunity for follow-up observations with targeted JWST NIRSpec spectroscopy, considering their positions within the Milky Way. A JWST NIRSpec + MIRI spectrum at 1 - $21\mu\text{m}$ of a $T_{\text{eff}} = 467\text{K}$ Y-dwarf was recently presented in Beiler et al. (2023). This source presented a

challenge to theoretical models, demonstrating the importance of increasing the number of these sources explored spectroscopically. Similarly, NIRSpec observations for three brown dwarfs found in the UNCOVER data (Langeroodi et al. 2023; Burgasser et al. 2023) were used to understand the atmospheres of these distant sources. Both sets of authors found evidence which suggests these sources are in the thick disk or halo. The existence of sources with these colors should be considered when selecting samples of high-redshift galaxies with signatures of black hole accretion.

This study demonstrates the importance of the NIR-Cam wavelength range of 2 - $5\mu\text{m}$ in selecting very faint, low-mass brown dwarfs. While extragalactic deep fields are designed to point outside the plane of our Galaxy to minimize stellar contamination, the usage of JWST deep observations to collect these sources has implications for the population of objects outside of the thick disk, which may be among the most metal-poor and oldest at these temperatures in the Galaxy. We expect that the large bounty of brown dwarf candidates found over the next several years will shed light on the history of star and planet formation in our Galaxy.

The authors want to thank the anonymous referee for their comments which greatly improved this manuscript. Additionally, the authors wish to thank Mark Marley for helpful discussions of brown dwarf atmospheric modeling. This work is based on observations made with the NASA/ESA/CSA James Webb Space Telescope, as part of JADES (Rieke, Marcia et al. 2023) and CEERS (Finkelstein, Steven et al. 2023). The data were obtained from the Mikulski Archive for Space Telescopes at the Space Telescope Science Institute, which is operated by the Association of Universities for Research in Astronomy, Inc., under NASA contract NAS5-03127 for JWST. These observations are associated with PID 1063, 1345, 1180, 1181, 1210, 1286, 1963, 1837, 1895, and 2738. Additionally, this work made use of the lux supercomputer at UC Santa Cruz which is funded by NSF MRI grant AST1828315, as well as the High Performance Computing (HPC) resources at the University of Arizona which is funded by the Office of Research Discovery and Innovation (ORDI), Chief Information Officer (CIO), and University Information Technology Services (UITS). We acknowledge support from the NIRCcam Science Team contract to the University of Arizona, NAS5-02015. Funding for this research was provided by the Johns Hopkins University, Institute for Data Intensive Engineering and Science (IDIES). W.B. acknowledges support by the Science and Technology Facilities Council (STFC), ERC Advanced Grant 695671 "QUENCH". REH acknowledges acknowledges support from the National Science Foundation Graduate Research Fellowship Program under Grant No. DGE-1746060. The research of CCW is supported by NOIR-Lab, which is managed by the Association of Universities for Research in Astronomy (AURA) under a cooperative agreement with the National Science Foundation. The authors are extremely grateful to the CEERS team lead by PI Steve Finkelstein and the FRESCO team led by PI Pascal Oesch for their work developing their observing programs and the zero-exclusive-access period on both. The authors also acknowledge Anton Koekemoer for the usage of CEERS HST data.

Facilities: JWST(NIRCcam, NIRSpec), HST(ACS, WFC3), Spitzer(IRAC)

Software: `astropy` (Astropy Collaboration et al. 2013, 2018, 2022), `astroquery` (Ginsburg et al. 2019), `matplotlib` (Hunter 2007), `numpy` (Harris et al. 2020), `scipy` (Virtanen et al. 2020), `Photutils` (Bradley et al. 2023), `EAZY` (Brammer et al. 2008).

REFERENCES

- Aganze, C., Burgasser, A. J., Malkan, M., et al. 2022, *ApJ*, 924, 114, doi: [10.3847/1538-4357/ac35ea](https://doi.org/10.3847/1538-4357/ac35ea)
- Arrabal Haro, P., Dickinson, M., Finkelstein, S. L., et al. 2023, *ApJL*, 951, L22, doi: [10.3847/2041-8213/acdd54](https://doi.org/10.3847/2041-8213/acdd54)
- Astropy Collaboration, Robitaille, T. P., Tollerud, E. J., et al. 2013, *A&A*, 558, A33, doi: [10.1051/0004-6361/201322068](https://doi.org/10.1051/0004-6361/201322068)
- Astropy Collaboration, Price-Whelan, A. M., Sipőcz, B. M., et al. 2018, *AJ*, 156, 123, doi: [10.3847/1538-3881/aabc4f](https://doi.org/10.3847/1538-3881/aabc4f)
- Astropy Collaboration, Price-Whelan, A. M., Lim, P. L., et al. 2022, *ApJ*, 935, 167, doi: [10.3847/1538-4357/ac7c74](https://doi.org/10.3847/1538-4357/ac7c74)
- Bañados, E., Venemans, B. P., Decarli, R., et al. 2016, *ApJS*, 227, 11, doi: [10.3847/0067-0049/227/1/11](https://doi.org/10.3847/0067-0049/227/1/11)
- Barro, G., Perez-Gonzalez, P. G., Kocevski, D. D., et al. 2023, arXiv e-prints, arXiv:2305.14418, doi: [10.48550/arXiv.2305.14418](https://doi.org/10.48550/arXiv.2305.14418)
- Beiler, S. A., Cushing, M. C., Kirkpatrick, J. D., et al. 2023, *ApJL*, 951, L48, doi: [10.3847/2041-8213/ace32c](https://doi.org/10.3847/2041-8213/ace32c)
- Bezanson, R., Labbe, I., Whitaker, K. E., et al. 2022, arXiv e-prints, arXiv:2212.04026, doi: [10.48550/arXiv.2212.04026](https://doi.org/10.48550/arXiv.2212.04026)
- Bouwens, R. J., Illingworth, G. D., Oesch, P. A., et al. 2015, *ApJ*, 803, 34, doi: [10.1088/0004-637X/803/1/34](https://doi.org/10.1088/0004-637X/803/1/34)
- Bradley, L., Sipőcz, B., Robitaille, T., et al. 2023, *astropy/photutils*: 1.8.0, 1.8.0, Zenodo, doi: [10.5281/zenodo.7946442](https://doi.org/10.5281/zenodo.7946442)
- Brammer, G. B., van Dokkum, P. G., & Coppi, P. 2008, *ApJ*, 686, 1503, doi: [10.1086/591786](https://doi.org/10.1086/591786)
- Bunker, A. J., Stanway, E. R., Ellis, R. S., & McMahon, R. G. 2004, *MNRAS*, 355, 374, doi: [10.1111/j.1365-2966.2004.08326.x](https://doi.org/10.1111/j.1365-2966.2004.08326.x)
- Bunker, A. J., Cameron, A. J., Curtis-Lake, E., et al. 2023, arXiv e-prints, arXiv:2306.02467, doi: [10.48550/arXiv.2306.02467](https://doi.org/10.48550/arXiv.2306.02467)
- Burgasser, A. J., Kirkpatrick, J. D., Cruz, K. L., et al. 2006, *ApJS*, 166, 585, doi: [10.1086/506327](https://doi.org/10.1086/506327)
- Burgasser, A. J., Kirkpatrick, J. D., Reid, I. N., et al. 2003a, *ApJ*, 586, 512, doi: [10.1086/346263](https://doi.org/10.1086/346263)
- Burgasser, A. J., Kirkpatrick, J. D., Brown, M. E., et al. 2002, *ApJ*, 564, 421, doi: [10.1086/324033](https://doi.org/10.1086/324033)
- Burgasser, A. J., Kirkpatrick, J. D., Burrows, A., et al. 2003b, *ApJ*, 592, 1186, doi: [10.1086/375813](https://doi.org/10.1086/375813)
- Burgasser, A. J., Gerasimov, R., Bezanson, R., et al. 2023, arXiv e-prints, arXiv:2308.12107, <https://arxiv.org/abs/2308.12107>
- Burningham, B., Smith, L., Cardoso, C. V., et al. 2014, *MNRAS*, 440, 359, doi: [10.1093/mnras/stu184](https://doi.org/10.1093/mnras/stu184)
- Calissendorff, P., De Furio, M., Meyer, M., et al. 2023, *ApJL*, 947, L30, doi: [10.3847/2041-8213/acc86d](https://doi.org/10.3847/2041-8213/acc86d)
- Casertano, S., Ratnatunga, K. U., & Bahcall, J. N. 1990, *ApJ*, 357, 435, doi: [10.1086/168933](https://doi.org/10.1086/168933)
- Casey, C. M., Kartaltepe, J. S., Drakos, N. E., et al. 2022, arXiv e-prints, arXiv:2211.07865, doi: [10.48550/arXiv.2211.07865](https://doi.org/10.48550/arXiv.2211.07865)
- Cruz, K. L., Burgasser, A. J., Reid, I. N., & Liebert, J. 2004, *ApJL*, 604, L61, doi: [10.1086/383415](https://doi.org/10.1086/383415)
- Curtis-Lake, E., Carniani, S., Cameron, A., et al. 2023, *Nature Astronomy*, 7, 622, doi: [10.1038/s41550-023-01918-w](https://doi.org/10.1038/s41550-023-01918-w)
- Cushing, M. C., Kirkpatrick, J. D., Gelino, C. R., et al. 2011, *ApJ*, 743, 50, doi: [10.1088/0004-637X/743/1/50](https://doi.org/10.1088/0004-637X/743/1/50)
- Dickinson, M., Giavalisco, M., & GOODS Team. 2003, in *The Mass of Galaxies at Low and High Redshift*, ed. R. Bender & A. Renzini, 324, doi: [10.1007/10899892_78](https://doi.org/10.1007/10899892_78)
- Dunlop, J. S., Abraham, R. G., Ashby, M. L. N., et al. 2021, PRIMER: Public Release IMaging for Extragalactic Research, JWST Proposal. Cycle 1, ID. #1837
- Dupuy, T. J., Liu, M. C., & Leggett, S. K. 2015, *ApJ*, 803, 102, doi: [10.1088/0004-637X/803/2/102](https://doi.org/10.1088/0004-637X/803/2/102)
- Eisenstein, D. J., Willott, C., Alberts, S., et al. 2023a, arXiv e-prints, arXiv:2306.02465, doi: [10.48550/arXiv.2306.02465](https://doi.org/10.48550/arXiv.2306.02465)
- Eisenstein, D. J., Johnson, B. D., Robertson, B., et al. 2023b, arXiv e-prints, arXiv:2310.12340, doi: [10.48550/arXiv.2310.12340](https://doi.org/10.48550/arXiv.2310.12340)
- Endsley, R., Stark, D. P., Chevallard, J., & Charlot, S. 2021, *MNRAS*, 500, 5229, doi: [10.1093/mnras/staa3370](https://doi.org/10.1093/mnras/staa3370)
- Endsley, R., Stark, D. P., Whittler, L., et al. 2022, arXiv e-prints, arXiv:2208.14999, doi: [10.48550/arXiv.2208.14999](https://doi.org/10.48550/arXiv.2208.14999)
- Finkelstein, S. L., Ryan, Russell E., J., Papovich, C., et al. 2015, *ApJ*, 810, 71, doi: [10.1088/0004-637X/810/1/71](https://doi.org/10.1088/0004-637X/810/1/71)
- Finkelstein, S. L., Bagley, M. B., Arrabal Haro, P., et al. 2022, *ApJL*, 940, L55, doi: [10.3847/2041-8213/ac966e](https://doi.org/10.3847/2041-8213/ac966e)
- Finkelstein, Steven, Bagley, Micaela, & Yang, Guang. 2023, Data from The Cosmic Evolution Early Release Science Survey (CEERS), STScI/MAST, doi: [10.17909/Z7P0-8481](https://doi.org/10.17909/Z7P0-8481)
- Franco, M., Akins, H. B., Casey, C. M., et al. 2023, arXiv e-prints, arXiv:2308.00751, doi: [10.48550/arXiv.2308.00751](https://doi.org/10.48550/arXiv.2308.00751)
- Fujimoto, S., Arrabal Haro, P., Dickinson, M., et al. 2023, *ApJL*, 949, L25, doi: [10.3847/2041-8213/acd2d9](https://doi.org/10.3847/2041-8213/acd2d9)
- Furtak, L. J., Zitrin, A., Plat, A., et al. 2022, arXiv e-prints, arXiv:2212.10531, doi: [10.48550/arXiv.2212.10531](https://doi.org/10.48550/arXiv.2212.10531)
- Giavalisco, M., Ferguson, H. C., Koekemoer, A. M., et al. 2004, *ApJL*, 600, L93, doi: [10.1086/379232](https://doi.org/10.1086/379232)

- Ginsburg, A., Sipőcz, B. M., Brasseur, C. E., et al. 2019, *AJ*, 157, 98, doi: [10.3847/1538-3881/aafc33](https://doi.org/10.3847/1538-3881/aafc33)
- Hainline, K. N., Hviding, R. E., Rieke, M., et al. 2020, *ApJ*, 892, 125, doi: [10.3847/1538-4357/ab7dc3](https://doi.org/10.3847/1538-4357/ab7dc3)
- Hainline, K. N., Johnson, B. D., Robertson, B., et al. 2023, arXiv e-prints, arXiv:2306.02468, doi: [10.48550/arXiv.2306.02468](https://doi.org/10.48550/arXiv.2306.02468)
- Harris, C. R., Millman, K. J., van der Walt, S. J., et al. 2020, *Nature*, 585, 357, doi: [10.1038/s41586-020-2649-2](https://doi.org/10.1038/s41586-020-2649-2)
- Holwerda, B. W., Bridge, J. S., Ryan, R., et al. 2018, *A&A*, 620, A132, doi: [10.1051/0004-6361/201832838](https://doi.org/10.1051/0004-6361/201832838)
- Hunter, J. D. 2007, *Computing in Science & Engineering*, 9, 90, doi: [10.1109/MCSE.2007.55](https://doi.org/10.1109/MCSE.2007.55)
- Illingworth, G. D., Magee, D., Oesch, P. A., et al. 2013, *ApJS*, 209, 6, doi: [10.1088/0067-0049/209/1/6](https://doi.org/10.1088/0067-0049/209/1/6)
- Ji, Z., Williams, C. C., Tacchella, S., et al. 2023, arXiv e-prints, arXiv:2305.18518, doi: [10.48550/arXiv.2305.18518](https://doi.org/10.48550/arXiv.2305.18518)
- Karalidi, T., Marley, M., Fortney, J. J., et al. 2021, *ApJ*, 923, 269, doi: [10.3847/1538-4357/ac3140](https://doi.org/10.3847/1538-4357/ac3140)
- Kirkpatrick, J. D., Reid, I. N., Liebert, J., et al. 1999, *ApJ*, 519, 802, doi: [10.1086/307414](https://doi.org/10.1086/307414)
- Kirkpatrick, J. D., Gelino, C. R., Faherty, J. K., et al. 2021, *ApJS*, 253, 7, doi: [10.3847/1538-4365/abd107](https://doi.org/10.3847/1538-4365/abd107)
- Kiwy, F., Faherty, J. K., Meisner, A., et al. 2022, *AJ*, 164, 3, doi: [10.3847/1538-3881/ac68e7](https://doi.org/10.3847/1538-3881/ac68e7)
- Labbé, I., van Dokkum, P., Nelson, E., et al. 2023, *Nature*, 616, 266, doi: [10.1038/s41586-023-05786-2](https://doi.org/10.1038/s41586-023-05786-2)
- Labbe, I., Greene, J. E., Bezanson, R., et al. 2023, arXiv e-prints, arXiv:2306.07320, doi: [10.48550/arXiv.2306.07320](https://doi.org/10.48550/arXiv.2306.07320)
- Langeroodi, D., Hjorth, J., & Zhang, Z. 2023, *Little Red Dots or Brown Dwarfs? NIRSpec Discovery of Three Brown Dwarfs Masquerading as NIRCам-Selected Highly-Reddened AGNs.* <https://arxiv.org/abs/2308.10900>
- Lodieu, N., Zapatero Osorio, M. R., Martín, E. L., Solano, E., & Aberasturi, M. 2010, *ApJL*, 708, L107, doi: [10.1088/2041-8205/708/2/L107](https://doi.org/10.1088/2041-8205/708/2/L107)
- Lorenzoni, S., Bunker, A. J., Wilkins, S. M., et al. 2013, *MNRAS*, 429, 150, doi: [10.1093/mnras/sts325](https://doi.org/10.1093/mnras/sts325)
- Marley, M. S., Saumon, D., Visscher, C., et al. 2021, *ApJ*, 920, 85, doi: [10.3847/1538-4357/ac141d](https://doi.org/10.3847/1538-4357/ac141d)
- Masters, D., McCarthy, P., Burgasser, A. J., et al. 2012, *ApJL*, 752, L14, doi: [10.1088/2041-8205/752/1/L14](https://doi.org/10.1088/2041-8205/752/1/L14)
- Matthee, J., Naidu, R. P., Brammer, G., et al. 2023, arXiv e-prints, arXiv:2306.05448, doi: [10.48550/arXiv.2306.05448](https://doi.org/10.48550/arXiv.2306.05448)
- Meisner, A. M., Caselden, D., Kirkpatrick, J. D., et al. 2020, *ApJ*, 889, 74, doi: [10.3847/1538-4357/ab6215](https://doi.org/10.3847/1538-4357/ab6215)
- Momcheva, I. G., Brammer, G. B., van Dokkum, P. G., et al. 2016, *ApJS*, 225, 27, doi: [10.3847/0067-0049/225/2/27](https://doi.org/10.3847/0067-0049/225/2/27)
- Morishita, T., Stiavelli, M., Chary, R.-R., et al. 2023, arXiv e-prints, arXiv:2308.05018, doi: [10.48550/arXiv.2308.05018](https://doi.org/10.48550/arXiv.2308.05018)
- Murray, D. N., Burningham, B., Jones, H. R. A., et al. 2011, *MNRAS*, 414, 575, doi: [10.1111/j.1365-2966.2011.18424.x](https://doi.org/10.1111/j.1365-2966.2011.18424.x)
- Nissen, P. E. 2004, in *Origin and Evolution of the Elements*, ed. A. McWilliam & M. Rauch, 154, doi: [10.48550/arXiv.astro-ph/0310326](https://doi.org/10.48550/arXiv.astro-ph/0310326)
- Nonino, M., Glazebrook, K., Burgasser, A. J., et al. 2023, *ApJL*, 942, L29, doi: [10.3847/2041-8213/ac8e5f](https://doi.org/10.3847/2041-8213/ac8e5f)
- Oesch, P. A., Bouwens, R. J., Illingworth, G. D., et al. 2012, *ApJ*, 759, 135, doi: [10.1088/0004-637X/759/2/135](https://doi.org/10.1088/0004-637X/759/2/135)
- Oesch, P. A., Brammer, G., Naidu, R. P., et al. 2023, *MNRAS*, doi: [10.1093/mnras/stad2411](https://doi.org/10.1093/mnras/stad2411)
- Oke, J. B. 1974, *ApJS*, 27, 21, doi: [10.1086/190287](https://doi.org/10.1086/190287)
- Pérez-González, P. G., Barro, G., Annunziatella, M., et al. 2023, *ApJL*, 946, L16, doi: [10.3847/2041-8213/acb3a5](https://doi.org/10.3847/2041-8213/acb3a5)
- Phillips, M. W., Tremblin, P., Baraffe, I., et al. 2020, *A&A*, 637, A38, doi: [10.1051/0004-6361/201937381](https://doi.org/10.1051/0004-6361/201937381)
- Rieke, Marcia, Robertson, Brant, Tacchella, Sandro, et al. 2023, *Data from the JWST Advanced Deep Extragalactic Survey (JADES), STScI/MAST,* doi: [10.17909/8TDJ-8N28](https://doi.org/10.17909/8TDJ-8N28)
- Robertson, B. E., Tacchella, S., Johnson, B. D., et al. 2023, *Nature Astronomy*, 7, 611, doi: [10.1038/s41550-023-01921-1](https://doi.org/10.1038/s41550-023-01921-1)
- Robin, A. C., Reylé, C., Derrière, S., & Picaud, S. 2003, *A&A*, 409, 523, doi: [10.1051/0004-6361:20031117](https://doi.org/10.1051/0004-6361:20031117)
- Ryan, R. E., J., & Reid, I. N. 2016, *AJ*, 151, 92, doi: [10.3847/0004-6256/151/4/92](https://doi.org/10.3847/0004-6256/151/4/92)
- Ryan, R. E., Thorman, P. A., Yan, H., et al. 2011, *ApJ*, 739, 83, doi: [10.1088/0004-637X/739/2/83](https://doi.org/10.1088/0004-637X/739/2/83)
- Schneider, A. C., Burgasser, A. J., Gerasimov, R., et al. 2020, *ApJ*, 898, 77, doi: [10.3847/1538-4357/ab9a40](https://doi.org/10.3847/1538-4357/ab9a40)
- Stanway, E. R., Bunker, A. J., & McMahon, R. G. 2003, *MNRAS*, 342, 439, doi: [10.1046/j.1365-8711.2003.06546.x](https://doi.org/10.1046/j.1365-8711.2003.06546.x)
- Tacchella, S., Eisenstein, D. J., Hainline, K., et al. 2023, arXiv e-prints, arXiv:2302.07234, doi: [10.48550/arXiv.2302.07234](https://doi.org/10.48550/arXiv.2302.07234)
- Topping, M. W., Stark, D. P., Endsley, R., et al. 2023, arXiv e-prints, arXiv:2307.08835, doi: [10.48550/arXiv.2307.08835](https://doi.org/10.48550/arXiv.2307.08835)
- Vanzella, E., Giavalisco, M., Dickinson, M., et al. 2009, *ApJ*, 695, 1163, doi: [10.1088/0004-637X/695/2/1163](https://doi.org/10.1088/0004-637X/695/2/1163)
- Virtanen, P., Gommers, R., Oliphant, T. E., et al. 2020, *Nature Methods*, 17, 261, doi: [10.1038/s41592-019-0686-2](https://doi.org/10.1038/s41592-019-0686-2)

Wang, P.-Y., Goto, T., Ho, S. C. C., et al. 2023, MNRAS, 523, 4534, doi: [10.1093/mnras/stad1679](https://doi.org/10.1093/mnras/stad1679)

Whitaker, K. E., Ashas, M., Illingworth, G., et al. 2019, ApJS, 244, 16, doi: [10.3847/1538-4365/ab3853](https://doi.org/10.3847/1538-4365/ab3853)

Wilkins, S. M., Stanway, E. R., & Bremer, M. N. 2014, MNRAS, 439, 1038, doi: [10.1093/mnras/stu029](https://doi.org/10.1093/mnras/stu029)

Williams, C. C., Tacchella, S., Maseda, M. V., et al. 2023, arXiv e-prints, arXiv:2301.09780, doi: [10.48550/arXiv.2301.09780](https://doi.org/10.48550/arXiv.2301.09780)

Zhang, Z. H., Burgasser, A. J., Gálvez-Ortiz, M. C., et al. 2019, MNRAS, 486, 1260, doi: [10.1093/mnras/stz777](https://doi.org/10.1093/mnras/stz777)